Manuscript submitted to
AIMS' Journals
Volume **X**, Number **0X**, XX **200X**

doi:10.3934/xx.xxxxxxx

pp. **X–XX**

Gaetana Gambino

Department of Mathematics and Computer Science, University of Palermo
Via Archirafi 34, 90123 Palermo, Italy

Valeria Giunta

School of Mathematics and Statistics, University of Sheffield
Hicks Building, Hounsfield Road, Sheffield, S3 7RH, UK

Maria Carmela Lombardo* and Gianfranco Rubino

Department of Mathematics and Computer Science, University of Palermo
Via Archirafi 34, 90123 Palermo, Italy

(Communicated by the associate editor name)

CROSS-DIFFUSION EFFECTS ON STATIONARY PATTERN FORMATION IN THE FITZHUGH-NAGUMO MODEL

Abstract. We investigate the formation of stationary patterns in the Fitz-Hugh-Nagumo reaction-diffusion system with linear cross-diffusion terms. We focus our analysis on the effects of cross-diffusion on the Turing mechanism. Linear stability analysis indicates that positive values of the inhibitor cross-diffusion enlarge the region in the parameter space where a Turing instability is excited. A sufficiently large cross-diffusion coefficient of the inhibitor removes the requirement imposed by the classical Turing mechanism that the inhibitor must diffuse faster than the activator. In an extended region of the parameter space a new phenomenon occurs, namely the existence of a double bifurcation threshold of the inhibitor/activator diffusivity ratio for the onset of patterning instabilities: for large values of inhibitor/activator diffusivity ratio, classical Turing patterns emerge where the two species are in-phase, while, for small values of the diffusion ratio, the analysis predicts the formation of out-of-phase spatial structures (named *cross-Turing patterns*). In addition, for increasingly large values of the inhibitor cross-diffusion, the upper and lower bifurcation thresholds merge, so that the instability develops independently on the value of the diffusion ratio, whose magnitude selects Turing or cross-Turing patterns. Finally, the pattern selection problem is addressed through a weakly nonlinear analysis.

1. **Introduction.** Diffusion driven instability is one of the fundamental mechanisms responsible of spatial pattern formation in different fields, such as ecology, biology and physics of plasma [10, 18, 24, 26, 46]. Classical Turing patterns are stationary-in-time spatially periodic structures which arise when two interacting substances spread at different diffusion ranges [50]. The Turing mechanism requires the coupling of a local self-enhancing reaction with a counter long-range process

2020 *Mathematics Subject Classification.* Primary: 35K57, 35B36, 35Q92; Secondary: 35B32, 37L10.

Key words and phrases. Cross-diffusion, FitzHugh-Nagumo, Turing instability, out-of-phase patterns, amplitude equations.

* Corresponding author: Maria Carmela Lombardo.

[19], and it is supported by reaction-diffusion systems where an autocatalytic activator interacts with a rapidly diffusing inhibitor [36]. More recently, the formation of spatial structures has been investigated in reaction-diffusion systems with nonlinear diffusion terms or with a non-diagonal matrix of diffusion coefficients (linear cross-diffusion), which account for the fact that a gradient in one species concentration can induce a flux of the other species [23, 42, 52, 56].

In this work, we shall investigate the impact of the linear cross-diffusion terms on the onset of stationary nonhomogeneous structures in the following FitzHugh-Nagumo (FHN)-type system [1, 2]:

$$\begin{aligned} \frac{\partial u}{\partial t} &= u(1-u^2) - (1-\beta u)v + \nabla^2 u + d_v \nabla^2 v\,, \\ \frac{\partial v}{\partial t} &= \varepsilon\,(\gamma u - v - a) + d_u \nabla^2 u + d\nabla^2 v, \end{aligned} \tag{1.1}$$

where $u(\mathbf{x},t)$ and $v(\mathbf{x},t)$ are the activator and the inhibitor species, respectively, being $\mathbf{x} \in \Omega \subset \mathbb{R}^n$ with $n = 1$ or 2. The parameter d is the ratio between the diffusion coefficients of v and u, respectively, and the parameters d_u and d_v are the cross-diffusion coefficients. The parameters $\varepsilon, \beta, \gamma$ and a characterize the local reaction dynamics: ε is the ratio between the typical timescales of the two species, γ and a control the number of intersections and the relative position of the nullclines, $0 \le \beta < 1$ is a small parameter which breaks the symmetry ($u \to -u, v \to -v, a \to -a$). The coefficient a is a real-valued parameter and all the other parameters are nonnegative. The system (1.1) will be supplemented with initial conditions and homogeneous Neumann boundary conditions.

The model (1.1) in the symmetric case $\beta = 0$ and with $d = d_u = d_v = 0$ is known as the FHN system and was introduced in [11, 41] to describe the neuronal communication mechanism along the nerve axon. The variable u, representing the electrical potential, is the excitatory variable and mimics the propagation of the action potential; the variable v acts as a controller related to the opening of the ion channels. Assuming a shorter length scale of coupling of v with respect to u, the diffusion of v is set equal to zero.

Although the FHN system originally goes back to the theoretical description of nerve pulse transmission, a model of the same class can be also derived in the context of population dynamics to reproduce prey-predator behavior in aquatic ecosystems. The details of the derivation are given in Appendix A. In this framework the variables (u, v) represent the small-amplitude deviations from the coexistence equilibrium and can therefore assume also negative values. The reaction kinetics proposed in (1.1) is a slightly modified form of the system (A.12)-(A.13) derived in Appendix A, in the sense that in (1.1) have been neglected cubic predation terms and a more general linear dependence in the v-nullcline has been introduced. The motivation for the choice of the reaction term as in (1.1) stems from the fact that it seems to be 'a kind of normal form' [44] and it has turned out to be very useful for the study of general features of spatiotemporal pattern formation.

In the modeling of chemical reactions or population dynamics, several authors have considered generalizations of the diffusion terms, choosing a positive value of the coefficient d in (1.1) to indicate a random diffusivity for the inhibitor [34, 53], or introducing cross-diffusion terms to account for evasion-pursuit mechanisms [30, 31, 37, 57, 60, 61, 62].

In this paper, we assume d, d_u and $d_v > 0$ to describe the following interaction: both species diffuse randomly; moreover, the u species tends to segregate from the v species and vice versa. In predator-prey systems, this choice of the cross-diffusion terms models a hunting strategy of the predator, consisting into heading to low density areas of the prey to maximize its hunting success, see [17, 47, 49]. Moreover, we focus on the case where the parameters of the reaction term are chosen in the monostable regime also known as oscillatory regime, leaving for future investigation the study in the excitable and bistable regimes (see the details of this classification in Section 2).

In absence of cross-diffusion, the study of classical Turing patterns for the monostable FHN system on regular domains is complete [63, 14]. In [14] the authors proved that the Turing bifurcation is always supercritical and derived the equations for the amplitude of the emerging patterns on 1D and 2D rectangular domains. In this work we prove that the presence of cross-diffusion terms significantly impacts on the pattern forming properties of the system. The first result is that the inclusion of cross-terms can relax or even remove the constraints imposed by the Turing mechanism on the diffusivity ratio. The well-established Turing condition for pattern formation, in fact, requires that, if the reaction kinetics is of activator-inhibitor form, the inhibitor must diffuse much faster than the activator. This restriction has been considered a major obstruction in explaining biological patterns since it makes the parameter region where patterning can occur typically too small to be compatible with the experimental robustness of patterns across a variety of scales and environments. The solutions proposed to overcome this problem usually consider an increased number of species [9, 27], domain growth [51], or the introduction of noise [54]. The inclusion in the model of cross-diffusion terms has also proven to be effective in enlarging the parameter region where diffusive instabilities arise, see [15, 32, 28, 21]. In this paper we show that the two cross-diffusion terms play opposite roles in the patterning process: while the presence of the inhibitor cross-diffusion helps in setting the instability by broadening the Turing space, an increase of the activator cross-diffusion reduces its width. Any positive value of the inhibitor cross-diffusion has the effect of lowering the self-diffusivity ratio instability threshold, whose value can be either greater, equal to, or less than unity, depending on the strength of the inhibitor cross-diffusion. Therefore, allowing for positive cross-diffusion of the inhibitor species removes the requirement of different diffusivities prescribed by the Turing mechanism.

A second important result, descending from the inclusion of cross-diffusion terms, is the occurrence of a new phenomenon, not observed in reaction-diffusion systems yet, namely, the existence of a double bifurcation threshold of d for the onset of diffusive instabilities. In fact, if the inhibitor cross-diffusion coefficient d_u is sufficiently large, the pattern forms for values of d external to the interval $[d_c^-, d_c^+]$, i.e. not only for values of the self-diffusion ratio *above* the threshold d_c^+ (as in the classical Turing mechanism), but also when the diffusion ratio d is *below* the lower threshold d_c^-. In the latter case, in fact, the diffusive instability is driven by the cross-diffusion of the inhibitor that escapes high concentration areas of the activator. One therefore needs a higher self-diffusion rate of the activator with respect to that of the inhibitor to maintain the pattern. This mechanism is opposite to what is prescribed by the classical Turing theory, which requires the inhibitor diffusing much faster than the activator. We have named *cross-Turing* patterns the stationary structures arising for small values of d that are originated by the presence of

the cross-diffusion terms. We show that the patterns arising for values of d *above* the threshold d_c^+ (Turing patterns) are in-phase, namely, the peaks and the troughs of the two species overlap on the spatial domain. The cross-Turing patterns, i.e. those originating *below*-threshold, are always out-of-phase, the concentration of the activator being higher in regions of low inhibitor concentration.

For very large values of the inhibitor cross-diffusion, a third scenario appears. The formation of the pattern is induced by the inhibitor cross-diffusion, whose strength completely removes any constraint on the value of the diffusivity ratio necessary for the diffusive instability. The pattern forms independently on the choice of the coefficient d, whose magnitude only selects the relative phase of species: while large values of d produce in-phase patterns, small values of d determine the onset of out-of-phase configurations.

Therefore, on the basis of the linear analysis, we identify three distinct regimes, characterized by increasing strengths of the inhibitor self-diffusion coefficient. The first regime (diffusion-dominated) is defined for small values of d_u: although the patterning process is regulated by the classical Turing mechanism, the presence of the cross-diffusion removes the differential diffusivity constraint and the formation of in-phase patterns is allowed also if the species diffuse at similar rates. For intermediate values of d_u, one has the second (competition) regime, where one can have Turing patterns if the self-diffusion ratio is above the upper threshold d_c^+, or cross-diffusion patterns for values of d below the lower threshold d_c^-. Finally, large d_u corresponds to the third regime (cross-diffusion dominated), where strong cross-diffusion of the inhibitor determines the instability, no matter of the values of the random dispersal rates of the species.

Remarkably, in a large region of the Turing space, the presence of cross-diffusion terms allows to obtain, with the same reaction kinetics, different phases of the species by only tuning the values of the self-diffusivities. This is a new result with respect to the Turing theory for two-species reaction-diffusion systems, by which the pattern phases are governed solely by the nature of the local interactions: reaction terms of the activator-inhibitor form originate only spatially overlapping (in-phase) patterns, while one needs a substrate-depleted-type reaction term to obtain mutually exclusive (out-of-phase) configurations. We have proved that including cross-diffusion in the model enables out-of-phase patterning in a simple two-species activator-inhibitor kinetics, without requiring multi-component systems [27]. We believe that this outcome could be used to model through activator-inhibitor systems mutually exclusive patterns, such as those observed within a cell [25, 29], or for the design of reaction-diffusion systems with desired patterning features [55].

Before concluding this Section, we briefly discuss the issue of the well-posedness of (1.1). The existence of global in time solutions to the FHN equations (1.1) has been addressed in [45], where, using the technique of contracting rectangles, the authors prove the global existence of solutions in the case $\beta = a = 0$ and in absence of the cross-diffusion terms (i.e. $d_u = d_v = 0$). Following the same lines as in [45], it is straightforward to extend the results of [45] to the system where non-symmetric term are included in the kinetics ($a, \beta \neq 0$), observing that a contracting rectangle can be found for the system (1.1) with $d_u = d_v = 0$ in the invariant domain $u < 1/\beta$. On the other hand, the presence of non-negative linear cross-diffusion terms makes the proof of the existence of globally defined solutions arduous and, in general reaction-diffusion systems, it has been achieved only when the reaction terms satisfy particular conditions, see [3, 43]. Indeed, the

kinetics in (1.1) does not verify the hypotheses of the theorems proved in [3, 43]. However, in this paper we will address near-to-equilibrium dynamics, therefore the behavior of the solutions is determined by their asymptotic representation in terms of amplitude functions [33, 22]. Moreover, all the performed numerical simulations confirm that the solutions exist from the time of initial perturbations to the final pattern, remaining next to the equilibrium.

The plan of the paper is the following. In Section 2, we classify the different dynamical regimes of the local FHN system and perform the linear stability analysis of the full system (1.1), so stating the conditions for the onset of Turing and cross-diffusion-induced (cross-Turing) instabilities. We also highlight the effect of the cross diffusion terms on the pattern forming mechanisms. In Section 3, we address the pattern selection problem and carry out the weakly nonlinear analysis. On one- and two-dimensional spatial domains, we derive the amplitude equations describing different bifurcation types and classify the stability of the corresponding steady states, leading to various spatial configurations. We also validate, through numerical simulations, the predictions of the linear analysis on the pattern phasing when nonlinearities are effective. Some conclusions are then drawn and directions for future work are given. Finally, for the reader's convenience, we have inserted three appendices, where technical derivations of some results presented in the paper are reported.

2. **Linear Analysis.**

In this Section we shall investigate the conditions for the onset of a Turing instability for the system (1.1). To this end, we shall first consider the reaction term of (1.1). We define:

$$f(u,v) = u(1-u^2) - (1-\beta u)v\,, \tag{2.1}$$

$$g(u,v) = \varepsilon\,(\gamma u - v - a)\,, \tag{2.2}$$

where $0 \leq \beta < 1$. The u-nullcline, namely the curve $f(u,v) = 0$, writes as:

$$v(u) = \frac{u(1-u^2)}{1-\beta u}\,. \tag{2.3}$$

In what follows, we shall restrict ourselves to the invariant region of the phase-space (u,v) such that $u < 1/\beta$. We shall denote by m and M the points of the (u,v)-plane corresponding to the local minimum and maximum of (2.3), respectively (see Figs. 1(a)-1(c)). We shall call 'inner branch' of the u-nullcline the portion of the curve that lies between m and M, and 'outer branches' the two remaining parts. Depending on the values of the parameters β, γ and a, the local dynamics of the FHN system (1.1) admits one or three homogeneous steady states (h.s.s.). We shall denote by 'inner equilibrium' an equilibrium point that lies on the inner branch of the u-nullcline and by 'outer equilibrium' an equilibrium point that lies on one of the outer branches. Therefore, we consider the following classification of the system (1.1), as given in [20], according to the possible relative positions of the u- and v-nullclines:

(i) *monostable case (or oscillatory case)*, when the local system in (1.1) admits a unique inner stable h.s.s. for $u < 1/\beta$, see Fig.1(a).

(ii) *excitable case*, when the local system in (1.1) has a unique outer stable h.s.s. for $u < 1/\beta$, see Fig.1(b).

(iii) *bistable case*, when the local system in (1.1) admits three h.s.s. for $u < 1/\beta$, two stable and one unstable, see Fig.1(c).

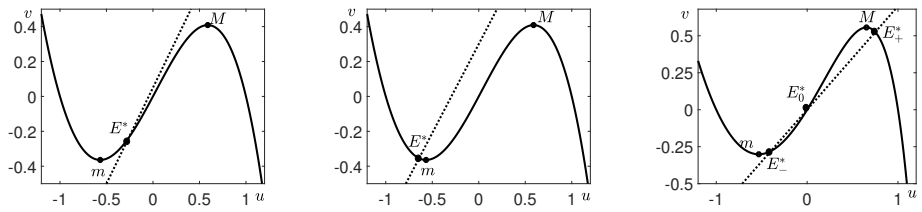

FIGURE 1. Nullclines of the local FHN system (1.1) in the monostable, excitable and bistable regime. (a) The monostable case, with $\varepsilon = 1, a = -0.05$, $\beta = 0.1$ and $\gamma = 1.1$. (b) The excitable case, with $\varepsilon = 1, a = -0.3$, $\beta = 0.1$ and $\gamma = 1.02$. (c) The bistable case, with $\varepsilon = 1, a = 0$, $\beta = 0.5$ and $\gamma = 0.7$. The labels m and M indicate the minimum and the maximum of the u-nullcline (2.3). The matrices give the signs of the derivatives f_u, f_v, g_u, g_v evaluated at the equilibrium point.

In this paper we shall analyze the formation of stationary patterns for the FHN system (1.1) in the *monostable* regime (case (i) above), so that the nullclines are of the form shown in Fig.1(a). We derive the conditions on the parameters under which the system (1.1) admits the unique monostable equilibrium $E^* \equiv (u^*, v^*)$ in Appendix B.

In the monostable regime, the signs of the partial derivatives f_u, f_v, g_u, g_v evaluated at the stable equilibrium points (and shown in Fig.1(a)) allow to classify the local interaction between u and v as of the activator-inhibitor type [40]. In fact, in the neighborhood of the stable equilibrium one has $g_u > 0$ and $f_v < 0$, so that u, the activator, promotes the growth of v, while v, the inhibitor, suppresses the increase of u. Besides, being $f_u > 0$, the u-species is self-activating, while, as $g_v < 0$, the v-species is self-inhibiting.

If we set $\mathbf{w} = (u - u^*, v - v^*)^T$, the linearization of the reaction terms of the system (1.1) in the neighborhood of E^* reads:

$$\mathbf{w}_t = K\mathbf{w}, \quad \text{where} \quad K = \begin{pmatrix} \varepsilon_H & -(1-\beta u^*) \\ \varepsilon\gamma & -\varepsilon \end{pmatrix}, \tag{2.4}$$

with $\varepsilon_H = 1 + \beta v^* - 3u^{*2}$. Recalling that $u < 1/\beta$, one has that $1 - \beta u^* > 0$. The equilibrium E^* is stable for the kinetics if the following two conditions hold:

$$\mathrm{tr(K)} = -\varepsilon + \varepsilon_H < 0, \tag{2.5}$$

$$\det(K) = \varepsilon\left[-\varepsilon_H + (1-\beta u^*)\,\gamma\right] > 0. \tag{2.6}$$

Let us discuss the sign of ε_H: upon differentiating the u-nullcline (2.3) with respect to u and evaluating all the quantities at the equilibrium E^*, one gets:

$$v'(u^*) = \frac{\varepsilon_H}{1-\beta u^*}. \tag{2.7}$$

Given that $1-\beta u^* > 0$, the sign of ε_H coincides with the sign of $v'(u^*)$. Since E^* is on the inner branch of the u-nullcline, $v'(u^*) > 0$ and $\varepsilon_H > 0$. Therefore, from the expressions of tr(K) and det(K) given in (2.5)-(2.6), one easily derives that the equilibrium can undergo both a Hopf bifurcation, when $\varepsilon_H = \varepsilon$, or a pitchfork bifurcation, when $\varepsilon_H = (1-\beta u^*)\,\gamma$. Since in this paper we are interested in the emergence of stationary structures, in what follows we shall assume $\varepsilon > \varepsilon_H$, so avoiding the occurrence of oscillations. Moreover, to satisfy (2.6), we shall always impose the following condition on the system parameters: $\gamma > \frac{\varepsilon_H}{1-\beta u^*}$.

Let us now perform the Turing bifurcation analysis of the reaction-diffusion system (1.1), whose linearization in the neighborhood of E^* is:

$$\frac{\partial \mathbf{w}}{\partial t} = \mathcal{L}\mathbf{w}, \tag{2.8}$$

where:

$$\mathcal{L} = K + D\nabla^2, \qquad D = \begin{pmatrix} 1 & d_v \\ d_u & d \end{pmatrix}, \tag{2.9}$$

and K is given in (2.4). To guarantee the well-posedness of the system (1.1) [48], hereafter we shall assume that:

$$\det(D) = d - d_u d_v > 0. \tag{2.10}$$

The steady state solution E^* undergoes a Turing bifurcation if it is stable with respect to spatially uniform perturbations and loses stability due to non-homogeneous perturbations. Namely, if we look for instability to perturbations proportional to $\cos(\mathbf{k}\cdot\mathbf{x})$, the linear stability analysis reduces to the following eigenvalue problem:

$$\lambda\,\mathbf{w} = \mathcal{M}(k^2)\,\mathbf{w}, \tag{2.11}$$

where

$$\mathcal{M}(k^2) = K - k^2 D, \tag{2.12}$$

and $k^2 = \mathbf{k}\cdot\mathbf{k}$. Instability is possible if $\Re(\lambda(k)) > 0$ for some $k \neq 0$, where $\lambda(k)$ is an eigenvalue of $\mathcal{M}(k^2)$, namely a solution of the following dispersion relation:

$$\lambda^2 + g\left(k^2\right)\lambda + h\left(k^2\right) = 0, \tag{2.13}$$

with:

$$\begin{aligned} h\left(k^2\right) &= \det(\mathcal{M}(k^2)) = \det(D)k^4 + qk^2 + \det(K), \\ g\left(k^2\right) &= -\mathrm{tr}(\mathcal{M}(k^2)) = k^2\mathrm{tr}(D) - \mathrm{tr}(K), \\ q &= -(K_{11}D_{22} + K_{22}D_{11}) + K_{12}D_{21} + K_{21}D_{12}, \end{aligned} \tag{2.14}$$

and K_{ij}, D_{ij} are the entries of the matrices K and D.
Under the hypothesis that the equilibrium E^* is stable for the kinetics, condition (2.5) holds so that the trace of $\mathcal{M}(k^2)$ is negative, i.e. $g\left(k^2\right) > 0$ for all k. Therefore, Turing instability can occur only if, due to the presence of the diffusion terms, one of the eigenvalues of the matrix $\mathcal{M}(k^2)$ crosses zero, namely if the curve $h(k^2) = \det(\mathcal{M}(k^2))$ assumes negative values for some k. Since $h(k^2)$ attains its minimum at:

$$k_c^2 = -\frac{q}{2\det(D)}, \tag{2.15}$$

the necessary conditions for yielding the Turing instability are the following [40]:

$$\begin{cases} q < 0\,, & \text{(2.16a)} \\ q^2 - 4\det(D)\det(K) \geq 0\,. & \text{(2.16b)} \end{cases}$$

Condition (2.16a) ensures that the minimum of $h(k^2)$ is attained at a positive value of k^2. Imposing that the minimum value of $h(k^2)$ is negative, so having a finite bandwidth of unstable wavenumbers k^2, one gets condition (2.16b). At the bifurcation, we require:

$$q^2 - 4\det(D)\det(K) = 0 \tag{2.17}$$

which, for fixed values of the other parameters, defines the critical values d_c of the bifurcation parameter d. In what follows we shall express the above given conditions (2.16a)-(2.16b) in terms of the parameters of the original system (1.1).

2.1. **Conditions for diffusive instability.** In this Subsection we shall derive the conditions for the onset of diffusive instabilities of the system (1.1), namely the conditions under which (2.10)-(2.16a)-(2.16b) are satisfied. We shall choose d as the bifurcation parameter.

In absence of the cross-diffusion terms, the qualitative form of the nullclines in the neighborhood of a monostable equilibrium (see Figs.1(a)) allows for the onset of Turing patterns. In fact, the activator-inhibitor type of the interaction between the species ($f_v\, g_u < 0$), is supplemented by the condition $f_u\, g_v < 0$, being the activator u self-activating and the inhibitor v self-inhibiting. Such a local dynamics satisfies the necessary conditions for the classical diffusion-driven instability. We shall show that generalizing the FHN model so as to include cross-diffusion terms produces new phenomena, enlarges the parameter region where instability may grow and originates two classes of qualitatively different spatially non-homogeneous solutions. We shall also highlight separately the role of varying d_u and d_v, showing that they have opposite influences on the width of the Turing region.

Let us consider (2.16a) first. Expliciting q as defined in (2.15) in terms of the system parameters, yields:

$$q = -\varepsilon_H d - (1 - \beta u^*)d_u + \varepsilon(1 + \gamma d_v). \tag{2.18}$$

When the equilibrium point E^* of the reaction terms (2.1)-(2.2) lies on the inner branch of the u-nullcline, one has that $\varepsilon_H > 0$. If one defines:

$$\bar{d} := \frac{1}{\varepsilon_H}(\varepsilon(1 + \gamma d_v) + (\beta u^* - 1)d_u), \tag{2.19}$$

it is easily seen that q vanishes for $d = \bar{d}$ and that condition (2.16a) is verified for $d > \bar{d}$, namely $\bar{d}$ is the threshold value of the bifurcation parameter d above which one gets a positive value of k_c^2. In the (d_u, d)-plane, for fixed d_v, this corresponds to the region above the straight line $d = \bar{d}$, see Figs.2(a)-2(b). Being $1 - \beta u^* > 0$ and $\varepsilon_H > 0$, the slope of $d = \bar{d}$ is negative while the intercept $I_c = \varepsilon(1 + \gamma d_v)/\varepsilon_H$ is positive (see Figs.2(a)-2(b)).

For fixed d_v, the quantity:

$$\delta_u^{(2)} := \frac{\varepsilon(1 + \gamma d_v)}{1 - \beta u^*} \tag{2.20}$$

is the value of d_u that makes $\bar{d} = 0$. A necessary condition to have a non-negative threshold of d for instability is therefore that $d_u \geq \delta_u^{(2)}$.

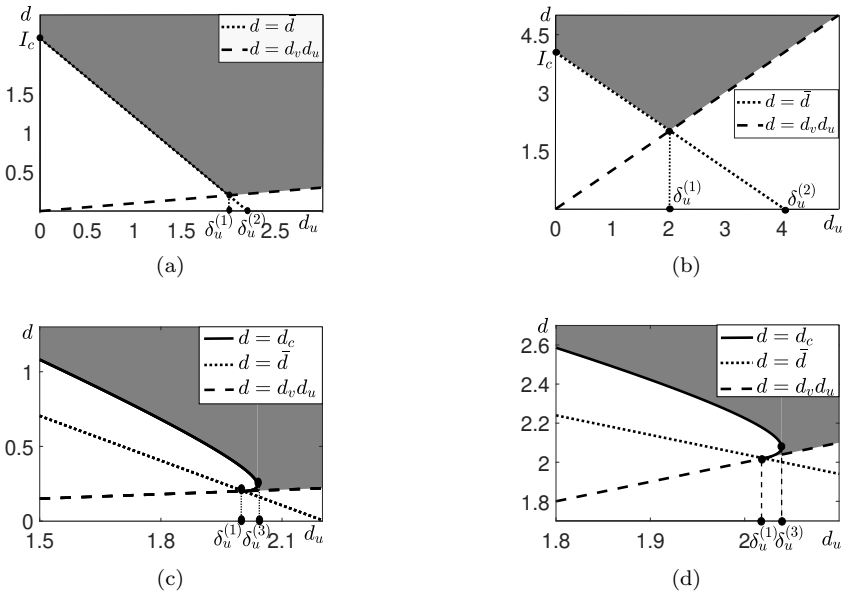

FIGURE 2. Geometrical representation of the conditions for the diffusive instability. (a)-(b) For two different choices of d_v, the dark gray regions in the (d_u, d)-plane delimited by the two straight lines $d = d_u\, d_v$ (dashed line) and $d = \bar{d}$ (dotted line) correspond to the fulfillment of conditions (2.10)-(2.16a). The other parameters are chosen as $\beta = 0.1, a = 0.0001, \gamma = 1.02, \varepsilon = 2$, so that $E^* = (0.0051, 0.0051)$. (a) $d_v = 0.1$, which gives $\delta_u^{(2)} = 2.2051, \delta_u^{(1)} = 2.0045, I_c = 2.2030$. (b) $d_v = 1$, which gives $\delta_u^{(2)} = 4.0421, \delta_u^{(1)} = 2.0201, I_c = 4.0382$. (c)-(d) For two different values of d_v, the gray shaded areas represent the diffusive instability regions in the (d_u, d)-plane, corresponding to the fulfillment of both (2.10)-(2.16a) and (2.16b). The boundaries of the Turing region are $d = d_c$, or $P(d) = 0$, (solid line) and $d = d_u d_v$ (dashed line). (c) The parameters are chosen as in (a). (d) The parameters are chosen as in (b).

We now impose the well-posedness condition (2.10): the two straight lines $d = d_v\, d_u$ and $d = \bar{d}$ expressing the marginality conditions of (2.10) and (2.16a), respectively, meet at the value $d_u = \delta_u^{(1)}$, with $\delta_u^{(1)}$ given by:

$$\delta_u^{(1)} := \frac{\varepsilon(1 + \gamma d_v)}{1 - \beta u^* + \varepsilon_H d_v}. \tag{2.21}$$

Hence, $\delta_u^{(1)}$ defines the abscissa of the lowest point of the region in the (d_u, d)-plane where one has both conditions (2.10) and (2.16a) verified. For fixed d_v, this region is represented by:

$$\begin{cases} d > \bar{d} & \text{for } d_u < \delta_u^{(1)} \\ d > d_v\, d_u & \text{for } d_u \geq \delta_u^{(1)} \end{cases} \tag{2.22}$$

which correspond to the area depicted in gray in Figs.2(a)-2(b). By inspection of (2.20)-(2.21), one easily verifies that $\delta_u^{(1)} \leq \delta_u^{(2)}$ for any non-negative d_v, where equality holds for $d_v = 0$. Upon increasing d_v, the straight line $d = \bar{d}$ is shifted upwards while the line $d = d_v\, d_u$ steepens, so that the intersection point moves up and, consequently, the width of the instability region is reduced (as it is also seen from the comparison of Figs.2(a)-2(b)).

Once (2.10) and (2.16a) are satisfied, let us now enforce condition (2.16b), where equality gives the threshold values for d. Written in terms of the system parameters, (2.16b) is expressed by the following second degree inequality:

$$P(d) := \varepsilon_H^2\, d^2 - 2d\, \left(\varepsilon_H^2 \bar{d}\ + 2\det(K)\right) + \varepsilon_H^2 \bar{d}^2 + 4\det(K) d_u d_v \geq 0. \tag{2.23}$$

The criticality in (2.23) is expressed in the (d_u, d)-plane by a parabola (see Figs.2(c)-2(d)), whose symmetry axis has the same slope of the line $d = \bar{d}$ (and is therefore negative) and whose intercept depends on d_v. The discriminant Δ of $P(d)$ reads:

$$\Delta = 4\det(K)(\det(K) + \varepsilon_H^2(\bar{d} - d_u d_v)). \tag{2.24}$$

Δ may assume either sign or vanish, depending on the values of the system parameters. In fact, while E^* is a stable equilibrium for the kinetics, by which $\det(K) > 0$, in the region given by (2.22) one has:

$$\begin{cases} \bar{d} > d_v\ d_u & \text{for } d_u < \delta_u^{(1)}, \\ \bar{d} \leq d_v\ d_u & \text{for } d_u \geq \delta_u^{(1)}. \end{cases} \tag{2.25}$$

To investigate the sign of Δ, we define the quantity:

$$\delta_u^{(3)} = \frac{\varepsilon_H\, \varepsilon(1 + \gamma d_v) + \det(K)}{\varepsilon_H(1 - \beta u^* + \varepsilon_H d_v)}, \tag{2.26}$$

which is the value of d_u that makes $\Delta = 0$. It is easily shown that, being the equilibrium stable, $\delta_u^{(1)} < \delta_u^{(3)}$.

We are now ready to derive the conditions under which (2.16b) is verified; we shall distinguish three different cases, depending on the value of the parameter d_u:

i) $d_u < \delta_u^{(1)}$ *(Diffusion-dominated regime)*

For $d_u < \delta_u^{(1)}$, by (2.22)-(2.25), one has $d \geq \bar{d} > d_v\, d_u$. Therefore $\Delta > 0$ and the quadratic polynomial $P(d)$ given by (2.23) admits two real roots, of whom the critical values for instability will be those that fall within the gray region depicted in Figs.2(a)-2(b), namely those that are greater than $\bar{d}$. It is straightforward to prove that only one of the two positive roots of $P(d)$, d_c, is greater than $\bar{d}$ (see also Figs.2(c)-2(d)), from which it follows that conditions (2.10) and (2.16a)-(2.16b) will be verified for $d \geq d_c$. To find the root d_c that lies above the threshold $\bar{d}$, in $P(d)$ we set $d = \bar{d} + \xi$. The resulting quadratic polinomial in ξ, given below by (2.27), admits only one real positive root ξ^+. Thus, choosing $d_u < \delta_u^{(1)}$, a Turing instability sets in for $d \geq d_c = \bar{d} + \xi^+$.

ii) $\delta_u^{(1)} \leq d_u \leq \delta_u^{(3)}$ *(Competition regime)*

In this case $\bar{d} < d_v\, d_u$, so that, to satisfy (2.16a) and (2.10) we have to take $d > d_v\ d_u$ (see (2.22)). Being $\delta_u^{(3)}$ the threshold value of d_u that makes $\Delta = 0$, for $d_u < \delta_u^{(3)}$ we have $\Delta > 0$ so that the quadratic polynomial $P(d)$ given by (2.23) still admits two real roots, say d_c^- and d_c^+. d_c^- and d_c^+ will be the bifurcation values of d if they both lie above the straight line $d = d_v d_u$ (see

Figs.2(c)-2(d)). It is straightforward to prove that this is the case: in fact, upon substituting $d = d_v d_u + \xi$ in (2.23), the resulting quadratic equation in ξ, given below by (2.30), by the Descartes' rule of signs admits the two roots ξ_1, ξ_2 with $0 < \xi_1 < \xi_2$. Hence, choosing $\delta_u^{(1)} \leq d_u \leq \delta_u^{(3)}$, a diffusive instability sets in for $d_v d_u < d \leq d_c^- = d_v d_u + \xi_1$ and for $d \geq d_c^+ = d_v d_u + \xi_2$ (see Figs.2(c)-2(d)).

iii) $d_u > \delta_u^{(3)}$ *(Cross-diffusion-dominated regime)*

In this region, being $\delta_u^{(1)} < \delta_u^{(3)} < d_u$, to satisfy (2.16a) and (2.10), we take $d > d_v d_u$. Moreover, the condition $d_u > \delta_u^{(3)}$ ensures that $\Delta < 0$ so that $P(d)$ never vanishes (see Figs.2(c)-2(d)) and (2.16b) is always satisfied. Therefore, the diffusion-driven instability occurs for all $d > d_v d_u$ that guarantee the well-posedness of the system (see Figs.2(c)-2(d)).

Hence, we have proved the following:

Theorem 2.1. *Given the system (1.1), let $\varepsilon_H > 0$, and let $E^* = (u^*, v^*)$ be the unique inner h.s.s. of the system, stable against spatially homogeneous perturbations. Let $\beta \geq 0$ be such that $1 - \beta u^* > 0$, and let d be the bifurcation parameter. Let $\bar{d}$, $\delta_u^{(1)}$ and $\delta_u^{(3)}$ be given by (2.19), (2.21) and (2.26), respectively, then:*

i) if $d_u < \delta_u^{(1)}$, the homogeneous equilibrium E^* undergoes a bifurcation whenever $d \geq d_c = \bar{d} + \xi^+$, where ξ^+ is the positive root of the following quadratic polynomial:

$$P_1(\xi) = \varepsilon_H^2 \xi^2 + 4\det(K)\xi - 4\det(K)(\bar{d} - d_u d_v). \tag{2.27}$$

The critical wavenumber is given by:

$$k_c = \sqrt{-\frac{q_c}{2\det(D_c)}}, \tag{2.28}$$

where:

$$q_c = -\varepsilon_H d_c - (1 - \beta u^*)d_u + \varepsilon(1 + \gamma d_v), \qquad \text{and} \qquad \det(D_c) = d_c - d_u d_v; \tag{2.29}$$

ii) if $\delta_u^{(1)} \leq d_u \leq \delta_u^{(3)}$, the homogeneous equilibrium E^* undergoes a bifurcation for

$$d_v d_u < d \leq d_c^- = d_v d_u + \xi_1 \qquad \text{and for} \qquad d \geq d_c^+ = d_v d_u + \xi_2,$$

where $0 < \xi_1 < \xi_2$ are the roots of the following polynomial:

$$\varepsilon_H^2 \xi^2 - 2\xi \left\{ \left[\varepsilon_H^2 d_v + \varepsilon_H (1 - \beta u^*) \right] (\delta_u^{(3)} - d_u) + \det(K) \right\} + \varepsilon_H^2 \left(\bar{d} - d_u d_v \right)^2. \tag{2.30}$$

At $d = d_c^\pm$ the critical wavenumber is given by:

$$k_c^\pm = \sqrt{-\frac{q_c^\pm}{2\det(D_c^\pm)}}, \tag{2.31}$$

where:

$$q_c^\pm = -\varepsilon_H d_c^\pm - (1 - \beta u^*)d_u + \varepsilon(1 + \gamma d_v), \qquad \text{and} \qquad \det(D_c^\pm) = d_c^\pm - d_u d_v; \tag{2.32}$$

iii) if $d_u > \delta_u^{(3)}$, *the homogeneous equilibrium* E^* *undergoes a bifurcation for all* $d > d_v d_u$. *For every fixed value of* d_u *and* d, *the most unstable wavenumber is given by:*

$$k = \sqrt{-\frac{q}{2\det(D)}}, \tag{2.33}$$

where D *and* q *are given in* (2.10) *and* (2.18), *respectively.*

2.2. **Discussion.** In the monostable case without cross-diffusion effects, the reaction kinetics of the FHN system allows for the onset of a Turing instability of the homogeneous steady state. The introduction of the cross-diffusion terms, as stated by Theorem 2.1, determines the existence of three different scenarios, each of whom, for a fixed value of d_v, is characterized by the value of the inhibitor cross-diffusion d_u.

The first regime, that we have called *diffusion-dominated*, corresponds to condition i) of Theorem 2.1: fixing d_v, if one chooses d_u *small* (in the sense indicated by i) of Theorem 2.1), a Turing instability can occur only for values of d greater then the threshold d_c. Hence, the insurgence of patterns is determined by the classical mechanism, subjected to the well-known constraint of a sufficiently large value of the ratio of the inhibitor/activator self-diffusion coefficients. Turing structures emerge where the u- and v-species are in-phase, as expected on the basis of the form of the linearized reaction kinetics. In the limit of vanishingly small values of d_u, one in fact recovers the known results obtained in absence of cross-diffusion. In this regime, the effect of the cross-diffusion is to lower the bifurcation value of d, that progressively reduces as d_u increases: as the inhibitor evades the activator, a larger self-diffusion coefficient of the activator is necessary to maintain the pattern with a net flux of activator from high density areas to less dense ones. The instability region is thus enlarged with respect to the classical case and Turing patterns can be observed also for $d \leq 1$. Therefore, upon varying the cross-diffusion coefficient, the requirement of *short-range activation/long-range inhibition* is relaxed and one can get stationary structures also with equal diffusivities or in the presence of *long-range activation/short-range inhibition*.

Fixing d_v and increasing the value of the cross diffusion parameter d_u, as expressed by condition ii) of Theorem 2.1, one has the second scenario, that we have called *competition* regime. Here the presence of the cross-diffusion terms generates the existence of a double bifurcation threshold, a phenomenon not prescribed by the classical Turing theory. In fact, in the interval $\delta_u^{(1)} \leq d_u \leq \delta_u^{(3)}$, one has two distinct regions of instability of the equilibrium: one above the upper branch of the parabola and one other below the lower branch (see Fig.3(a)). If the inhibitor self-diffusion is predominant, i.e. when $d \geq d_c^+$, one has a Turing bifurcation that generates in-phase patterns where, as in the classical case, the activator peak is bigger than the inhibitor peak (see Fig.3(b)). As in the *diffusion-dominated* case, in above-threshold instabilities the effect of the inhibitor cross-diffusion term is to lower the bifurcation value, so allowing for pattern formation also for values of the diffusivity ratio less than unity. Conversely, for values of the self-diffusion ratio d *below-threshold* (i.e. when $d \leq d_c^-$), the diffusive instability mechanism is driven by the cross-term and one needs larger self-dispersal rate of the activator with respect to that of the inhibitor for the development of the pattern. With the inhibitor evading the activator, regions of high density of the activator correspond to low-density of the inhibitor, resulting in out-of-phase patterns (see Fig.3(c)). This can

be proved by the linear analysis as follows: the pattern grows along the unstable manifold associated to the positive eigenvalue of the linearized dynamics. The explicit form of the corresponding eigenvector (given by formula (3.5) below) shows that the components of the eigenvector $\boldsymbol{\varrho}$ have opposite signs, corresponding to out-of-phase spatial distribution of the species. The numerical simulations of the nonlinear system (1.1) performed on $1D$ and $2D$ spatial domains demonstrate that the phase relationship coming from the linear analysis are maintained also when the nonlinearities come into play, as shown in Figs.3-4-6 and in all the snapshots of the cross-Turing pattern shown in Section 3.

It should be noted that, for a fixed value of d_u, the bifurcations occurring at $d = d_c^+$ and $d = d_c^-$ have, in general, different values of the critical mode, that we have denoted by k_c^+ and k_c^-, respectively (see Fig.3(b)-3(c)). As one moves along the above and lower branch of the parabola, respectively, towards the point where $d_u = \delta_u^{(3)}$, k_c^+ and k_c^- converge to a unique value of the critical mode and, while the peaks of the activator do not change significantly their size as d_u is increased, the height of the inhibitor maxima progressively shrinks. At the tangency point of the parabola with the line $d_u = \delta_u^{(3)}$, the pattern consists of localized regions of activator immersed in a uniform distribution of the inhibitor, corresponding to the value of the homogeneous equilibrium, see Fig.4.

Finally, the third regime, that we have named *cross-diffusion-dominated*, is attained for further increased values of the cross diffusion parameter d_u, as expressed by condition *iii)* of Theorem 2.1. As d_u crosses the value $\delta_u^{(3)}$, the instability occurs for all d satisfying the well-posedness condition. Therefore, for fixed d_u, the value of the self-diffusion coefficient d is irrelevant for the onset of the instability: there is no critical value of the bifurcation parameter and the instability sets in with fastest growing wavenumber given by (2.33). In this region, for fixed d_u, the effect of choosing different values of d determines the qualitative form of the pattern, discerning whether the patterns of the two species are in-phase (for high values of d), or out-of-phase (for small values of d). A quantitative threshold can be computed close to the line $d_u = \delta_u^{(3)}$, where the linear theory prescribes the emergence of Turing or cross-Turing patterns, depending on choosing the parameters above or below the curve:

$$d = \frac{(1-\beta u^*)d_u + \varepsilon(\gamma d_v - 1)}{2\varepsilon\gamma - \varepsilon_H d_u}\, d_u, \tag{2.34}$$

as shown in Fig.3(a). If the parameters are chosen along the curve (2.34), only the u-species stabilizes on a periodic structure, while the v-species stays homogeneously distributed within the domain at the value of the homogeneous equilibrium.

In all the three regimes, it is the inhibitor cross-diffusion d_u that is responsible for the occurrence of the phenomena above exposed: as stated by Theorem 2.1, the role played by the activator cross-diffusion d_v is to regulate the thresholds at which transitions from one regime to another occur, and the bifurcation values of d. This can be seen as follows. When both the cross-diffusion term vanish, one recovers the classical Turing mechanism: the instability sets in along the half-line on the d-axis whose lowermost value is given by the intercept I_c of the straight line $d = \bar{d}$ evaluated for $d_u = d_v = 0$. If one maintains $d_u = 0$ and increases d_v, the intercept of the line $d = \bar{d}$ moves upwards, so reducing the d-interval where the instability can grow. Instead, with $d_v = 0$, the conditions (2.16a)-(2.10) are satisfied for all positive values of d_u in the region of the (d_u, d)-plane given by (2.22), where one can then impose (2.16b). It is therefore the presence of the inhibitor cross-term

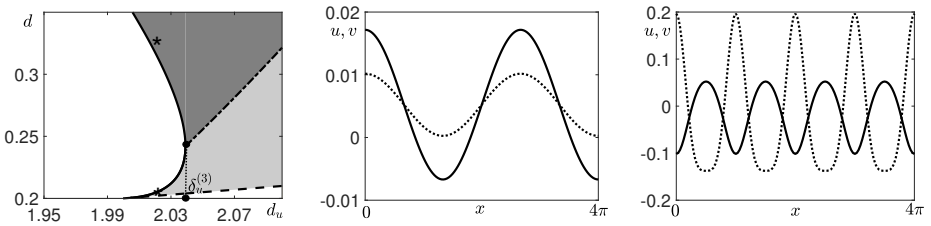

(a) (b) (c)

FIGURE 3. The kinetics parameters are chosen as in Fig.2(a). (a) The dark-gray and light-gray region indicate the presence of Turing and cross-Turing patterns, respectively, separated by the dash-dot curve expressed by (2.34). The dashed line marks the boundary above which $d > d_u d_v$. (b) Turing pattern obtained by the numerical simulation of the system (1.1), with $d_v = 0.1$, $d_u = 2.0194$ and $d = 0.32 > d_c^+ = 0.3191$ (so that $k_c^+ = 0.75$), corresponding to the point marked by an asterisk in (a). The profile of the activator (inhibitor) is represented by a solid (dotted) line. (c) Cross-Turing pattern obtained by the numerical simulation of the system (1.1) with $d_v = 0.1$, $d_u = 2.0194$ and $d = 0.20423 < d_c^- = 0.20432$ (so that $k_c^- = 2$), corresponding to the point marked by a plus sign in (a). The profile of the activator u (inhibitor v) is represented by a solid (dotted) line.

that determines the existence of the three different regimes and the presence of the cross-diffusion-induced bifurcation. An increase of d_v, for fixed d_u, induces a shrink of the instability region, as it can be seen also from the comparison of Figs.2(c)-(d): increasing d_v in fact moves upwards the line $d = \bar{d}$ and steepens the line $d = d_v\, d_u$. On the other hand, for fixed d_v, any increase in $d_u \in (0, \delta_u^{(3)}]$ makes it larger the d-interval where one has instability. For d_u larger that $\delta_u^{(3)}$, one then has instability for all the values of d that guarantee the well-posedness of the system.

To conclude this Section, we remark that generalizing the diffusion matrix with the introduction of inhibitor cross-diffusion removes the requirement of *short-range activation/long-range inhibition*, allowing the formation of patterns when one has *long-range activation/short-range inhibition* and also for comparable values of the diffusion coefficients. Therefore, fixing all the parameters and varying the ratio of the two diffusivities gives rises to qualitatively different configurations (see Fig.3). Finally, the generalized diffusion matrix determines a noteworthy phenomenon: namely, the existence of zones in the parameter space where the instability may lead to spatially localization of the activator within a nearly uniform distribution of the inhibitor.

3. **Pattern selection problem and amplitude equations.** In this Section we shall perform a weakly nonlinear analysis aimed at predicting the shape and the amplitude of the stationary patterns supported by the FHN system (1.1).

The analysis in the monostable regime, in the symmetric case ($\beta = a = 0$) and without cross diffusion terms ($d_u = d_v = 0$), has been carried out in [14]. Here,

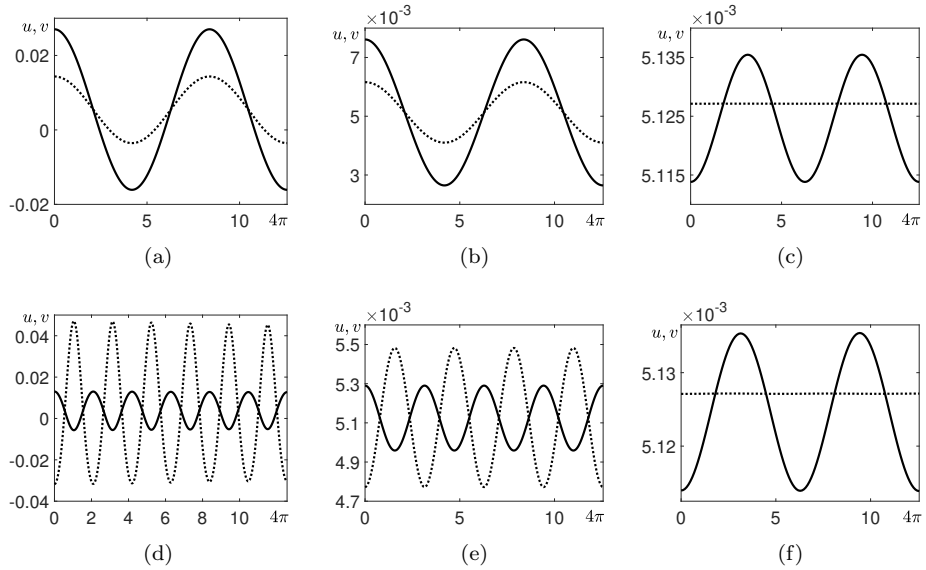

FIGURE 4. (a)-(b)-(c) Turing patterns observed along the upper branch of the bifurcation parabola. (d)-(e)-(f) Cross-Turing patterns observed along the lower branch of the bifurcation parabola. The parameters are chosen as in Fig.2(a). The profile of the activator u (inhibitor v) is represented by a solid (dotted) line. (a) $d_u = 2.012$ and $d = 0.3398 > d_c^+ = 0.3364$, so that $k_c^+ = 0.7$. (b) $d_u = 2.0198$ and $d = 0.3213 > d_c^+ = 0.3181$, so that $k_c^+ = 0.7568$. (c) $d_u = 2.0385$ and $d = 0.2527 > d_c^+ = 0.2553$, so that $k_c^+ = 0.9$. (d) $d_u = 2.0198$ and $d = 0.201689 < d_c^- = 0.2017$, so that $k_c^- = 3$. (e) $d_u = 2.0194$ and $d = 0.2040 < d_c^- = 0.2044$, so that $k_c^- = 1.9881$. (f) $d_u = 2.0385$ and $d = 0.2319 < d_c^- = 0.2324$, so that $k_c^- = 1.07$.

we shall include in our study symmetry-breaking ($\beta \neq 0, a \neq 0$) and cross-diffusion effects.

3.1. **One-dimensional domain.** Let μ, defined by $\mu^2 = |d - d_c|/d_c$, be the control parameter that measures the distance from the bifurcation threshold. We shall consider the following asymptotic expansions for $\mathbf{w}, t$ and d:

$$\mathbf{w} = \mu \mathbf{w}_1 + \mu^2 \mathbf{w}_2 + \mu^3 \mathbf{w}_3 + \dots, \tag{3.1}$$

$$t = t + \mu T_1 + \mu^2 T_2 + \dots, \tag{3.2}$$

$$d = d_c + \mu d^{(1)} + \mu^2 d^{(2)} + \mu^3 d^{(3)} \dots, \tag{3.3}$$

where $d^{(i)} > 0,\ i = 1, 2, \dots$ for Turing bifurcation and $d^{(i)} < 0,\ i = 1, 2, \dots$ for the cross-diffusion bifurcation. Substituting the above expressions (3.1)-(3.3) into the system (1.1) and collecting the terms at each order in μ, we find a sequence of equations for the coefficients $\mathbf{w}_i$. At $O(\mu)$ we obtain the following linear homogeneous problem:

$$\mathcal{L}^c \mathbf{w}_1 = 0, \tag{3.4}$$

where $\mathcal{L}^c$ is the linear operator in (2.9) evaluated at $d = d_c$. On a one-dimensional domain, the solution of (3.4) satisfying the Neumann boundary conditions is:

$$\begin{aligned} \mathbf{w}_1 &= A(T_1, T_2, \dots)\boldsymbol{\varrho}\cos(k_c x), \\ \boldsymbol{\varrho} &= \begin{pmatrix} 1 \\ M \end{pmatrix} \in Ker(K - k_c^2 D^c), \qquad M = \frac{\varepsilon_H - k_c^2}{1 - \beta u^* + k_c^2 d_v}, \end{aligned} \tag{3.5}$$

where A is an unknown amplitude and k_c is defined in (2.15).

The problem at $O(\mu^2)$ reads as:

$$\mathcal{L}^c \mathbf{w}_2 = \mathbf{F}, \tag{3.6}$$

where $\mathbf{F}$, whose explicit expression is given in (C.1), automatically satisfies the Fredholm alternative; thus the solution $\mathbf{w}_2$ can be easily computed.

In order to solve the problem $\mathcal{L}^c \mathbf{w}_3 = \mathbf{G}$ at $O(\mu^3)$, the compatibility condition must be imposed, which leads to the following Stuart-Landau equation for the amplitude A:

$$\frac{dA}{dT_2} = \sigma A - L A^3, \tag{3.7}$$

where $\sigma > 0$ and the Landau coefficient L are computed in terms of the parameters of the FHN system (1.1). The details of the procedure leading to Eq.(3.7) and the explicit expressions of $\sigma > 0$ and L are given in Appendix C. In the above equation (3.7), the sign of L characterizes the bifurcation, discerning between a supercritical and a subcritical transition. If the system parameters are chosen in such a way that L is positive, then the bifurcation is supercritical: past the threshold, Eq.(3.7) admits two symmetric stable steady states that provide the amplitude of the emerging pattern. Besides, the transition from the stable homogeneous equilibrium to the periodic-in-space stable solution is continuous as the bifurcation parameter crosses the threshold. Instead, if L is negative, the transition is subcritical: in this case, as the homogeneous equilibrium loses stability, one has an abrupt jump to the patterned state that remains stable when the bifurcation parameter is restored. In this case, past the threshold, Eq.(3.7) does not admit any stable solution and, therefore, is not able to capture the amplitude of the resulting pattern. In the subcritical case, the analytical approximation of the emerging solution then requires that one pushes the asymptotic expansion up to higher orders, see [15, 12]. The explicit analysis of the sign of L given by (C.6) as a function of all the system parameters is extremely difficult. We have therefore numerically computed L and shown the corresponding results in Fig.5.

In Fig.5(a) the black, gray and dark gray regions correspond to cross-Turing subcritical bifurcation, cross-Turing supercritical bifurcation and Turing supercritical bifurcation, respectively. We observe that, for a fixed value of d_v, the Turing bifurcation is always supercritical while the cross-diffusion patterns may arise as a consequence of either a sub- or a super-critical transition, depending on the value of d_u. Namely, the cross-diffusion pattern is subcritical for values of d_u slightly above the threshold $\delta_u^{(1)}$ and for small values of the self-diffusivities ratio d. In the subcritical region, in fact, although the inhibitor cross-diffusion coefficient is big enough to excite the instability, the high value of the activator self-diffusion coefficient locally stabilizes the homogeneous equilibrium. Therefore, a perturbation of sufficiently large amplitude is required for the settlement of a far-from-equilibrium pattern. As the value of d_u increases, the destabilizing effect of the cross-diffusion

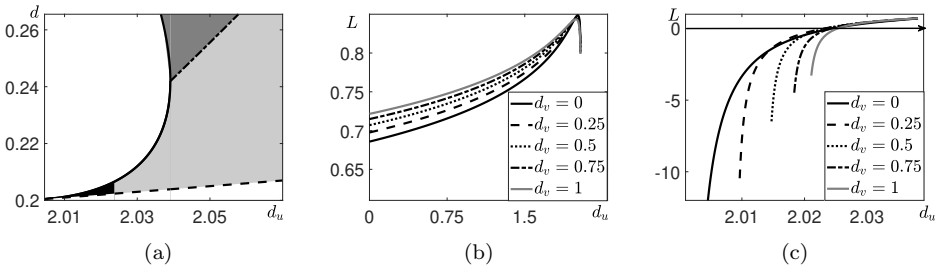

FIGURE 5. (a) Bifurcation diagram of the system (1.1) in the (d_u, d)-plane as given by the WNL theory. The black, gray and dark gray regions correspond to cross-Turing subcritical bifurcation, cross-Turing supercritical bifurcation and Turing supercritical bifurcation, respectively. The dashed line marks the boundary above which $d > d_u d_v$. The dash-dot curve, expressed by (2.34), that separates Turing from cross-Turing patterns is also reported. The parameters are chosen as in Fig.2. (b) Turing instability for $d \geq d_c^+$: graph of the coefficient L of the amplitude equation (3.7) versus d_u for different choices of d_v. The kinetic parameter are chosen as in (a). (c) Cross-Turing instability for $d \leq d_c^-$: graph of the coefficient L of the amplitude equation (3.7) versus d_u for different choices of d_v. The kinetic parameter are chosen as in (a).

on the homogeneous state progressively grows allowing for a supercritical transition. The sign of the Landau coefficient L appearing in (3.7) as a function of d_u and for different values of d_v is shown in Figs.5(b)-5(c) for the Turing and cross-Turing case, respectively: the graphs confirms that, as d_v varies, the Turing bifurcation remains supercritical while the cross-diffusion pattern can be super-critical or subcritical, depending on the choice of the cross-diffusion coefficients.

From the above analysis, one can suitably predict the emerging solution of the system (1.1) on a one-dimensional domain as follows:

Asymptotic solution in the neighborhood of a monostable equilibrium:
Given the system (1.1), let $E^* = (u^*, v^*)$ be the unique h.s.s. of the system. Let E^* be stable against spatially homogeneous perturbations and let E^* undergo a diffusive bifurcation at $d = d_c$. If:

i) the distance from the bifurcation value is small enough such that k_c is the only unstable mode admitted by the boundary conditions;

ii) the coefficient L of the Stuart-Landau equation (3.7) is positive, i.e. the bifurcation is supercritical;

then the asymptotic solution of the system (1.1) on a one dimensional domain $[0, L]$ is:

$$\mathbf{w} = \mu A_\infty \boldsymbol{\varrho} \cos(k_c x) + O(\mu^2), \tag{3.8}$$

where A_∞ is the stable steady state of the equation (3.7) and $\boldsymbol{\varrho}$ is defined in (3.5).

Formula (3.8) yields the asymptotic form of the pattern in the two cases of diffusive instabilities at a monostable equilibrium stated in Theorem 2.1, namely in the Turing and in the cross-Turing case, the only difference in the asymptotic

analysis being the choice of the sign of the coefficients $d^{(i)}$ appearing in (3.3). We do not report any numerical simulation of the pattern on one-dimensional domains as predicted by (3.8) as the case of rolls will be treated and illustrated below on two-dimensional domains.

To conclude this Subsection, we recall the fact that, if the bifurcation is subcritical, higher orders of the asymptotic expansion (3.1)-(3.3) need to be computed in order to capture the value of the saturated amplitude.

3.2. **Two-dimensional domain.** On a two-dimensional rectangular domain $\Omega \equiv [0, L_x] \times [0, L_y]$, the solution to the linearized system (2.8) satisfying the Neumann boundary conditions has the following form:

$$\mathbf{w} = \sum_{m,n \in \mathbb{N}} \mathbf{f}_{mn} e^{\lambda(k^2_{mn})t} \cos(\phi x) \cos(\psi y), \tag{3.9}$$

with:

$$\phi = \frac{m\pi}{L_x}, \quad \psi = \frac{n\pi}{L_y}, \qquad m, n \in \mathbb{N}, \tag{3.10}$$

where $\mathbf{f}_{mn}$ are the Fourier coefficients of the initial conditions and λ are the eigenvalues computed using the dispersion relation (2.13). The corresponding critical wavenumber k_c, computed as in (2.15), must satisfy the following condition:

$$k_c^2 = \phi^2 + \psi^2, \tag{3.11}$$

where ϕ and ψ are defined as in (3.10). In what follows, we will assume that there exists only one unstable wavenumber k_c admitted by the boundary conditions in the spatial domain Ω. The diffusive bifurcation is *regular* or *degenerate* depending on the existence of one or two mode pairs of integers (m, n) satisfying conditions (3.10)-(3.11), respectively. The WNL analysis will predict the emerging solution of the original system (1.1) as formulated below.

CASE 1 (Regular):
Asymptotic solution at a regular diffusive bifurcation in the neighborhood of a monostable equilibrium.
Given the system (1.1), let $E^* = (u^*, v^*)$ be the monostable h.s.s. of the system. Let E^* be stable against spatially homogeneous perturbations and let E^* undergo a diffusive bifurcation at $d = d_c$. If:

- *i) the distance μ from the bifurcation value is small enough such that k_c is the only unstable wavenumber admitted by the boundary conditions;*
- *ii) in the rectangular domain $\Omega \equiv [0, L_x] \times [0, L_y]$ there exists only one mode pair of integers (m, n) defined as in (3.10) and satisfying condition (3.11);*
- *iii) the coefficient L of the Stuart-Landau equation as in (3.7) is positive, i.e. the bifurcation is supercritical;*

then the asymptotic solution of the system (1.1) on the rectangular domain Ω is:

$$\mathbf{w} = \mu A_\infty \boldsymbol{\varrho} \cos(\phi x) \cos(\psi y) + O(\mu^2), \tag{3.12}$$

where A_∞ is the stable steady state of the equation (3.7), $\boldsymbol{\varrho}$ is given in (3.5), ϕ and ψ are defined as in (3.10)-(3.11).

In what follows we shall provide some numerical simulations that illustrate the patterns arising close to the cross-Turing bifurcation threshold on two-dimensional spatial domains. All the numerical simulations of system (1.1) reported in this Section are obtained using a second-order Runge- Kutta time-stepping scheme with

$dt = 10^{-2}$ and, for space discretization, a Fourier spectral scheme with 256×256 modes. The initial conditions are a random perturbation of the homogeneous equilibrium state of order 10^{-4}. We have assumed that the solution has attained a stationary state (and reported the corresponding spatial configuration) when $\max_{i,j} |\mathbf{w}(i,j,t(end)) - \mathbf{w}(i,j,t(end-1))| < 10^{-7}$.

According to Theorem 2.1, when the parameters are chosen in the competition regime ($\delta_u^{(1)} \leq d_u \leq \delta_u^{(3)}$), the homogeneous equilibrium may undergo to a Turing or to a cross-Turing bifurcation, depending on the value of the bifurcation parameter d. In Fig.6 we show the solution of the system (1.1) when the monostable equilibrium loses stability through a regular cross-Turing bifurcation at $d = d_c^- = 0.2198$. The parameters are chosen so that the hypotheses of Theorem 2.1 (competition regime and cross-Turing bifurcation) and the conditions $i) - iii)$ of Case 1 are satisfied. In the square domain $[0, 4\sqrt{2}\pi/k_c] \times [0, 4\sqrt{2}\pi/k_c]$, the only unstable mode $k_c^- \approx 1.2356$ admitted by the boundary conditions corresponds to the unique mode pairs $(m,n) = (4,4)$ satisfying the condition (3.11). The emerging cross-Turing pattern is well approximated by (3.12) with $A_\infty = 0.4866$, unique stable equilibrium of the Stuart-Landau equation (3.7). The spectra of the numerical solution of the system (1.1), reported in Fig.6(b)-6(d), show the agreement with the expected solution, being $(4,4)$ the couple of modes with higher amplitude. The mode pairs $(8,0)$ and $(0,8)$ are sub-harmonics which can be predicted at order ε^2.

We do not show the simulation reproducing the Turing pattern, obtained for the same parameter values of Fig.6 except d, leading, close to $d = d_c^+$, to in-phase spatially periodic species concentration with a different value of k_c^2.

We conclude the study of the diffusive instability at a regular bifurcation showing in Fig.7 a numerical simulation of a subcritical case. We recall that, in the case of a subcritical transition, the asymptotic procedure developed here does not apply since, to predict shape and amplitude of the emerging structures, one should push the analysis to higher orders (see details in [12]). Indeed, for the parameter set chosen in Fig.7, the linear analysis yields $k_c^- \approx 2.4495$ as the most unstable wavenumber, that corresponds to the unique couple of integers $(m,n) = (2,2)$ satisfying the condition (3.11). Instead, the spectra of the stationary configurations emerging from a random perturbation of the homogeneous equilibrium reveal the presence of several different modes, whose amplitude is comparable with the one of $(2,2)$.

CASE 2 (Mixed-mode):
Asymptotic solution at a degenerate diffusive bifurcation in the neighborhood of a monostable equilibrium, non-resonant case.
Given the system (1.1), let $E^* = (u^*, v^*)$ be the monostable h.s.s. of the system. Let E^* be stable against spatially homogeneous perturbations and let E^* undergo a diffusive bifurcation at $d = d_c$. If:

- *i) the distance μ from the bifurcation value is small enough such that k_c is the only unstable wavenumber admitted by the boundary conditions;*
- *ii) in the rectangular domain $\Omega \equiv [0, L_x] \times [0, L_y]$ there exists two mode pairs of integers $(m_i, n_i), i = 1,2$ defined as in (3.10) and satisfying condition (3.11);*
- *iii) the following non-resonance conditions hold:*

$$\begin{array}{ccc} \phi_i + \phi_j \neq \phi_j & \text{or} & \psi_i - \psi_j \neq \psi_j, \\ & \text{and} & \\ \phi_i - \phi_j \neq \phi_j & \text{or} & \psi_i + \psi_j \neq \psi_j, \end{array} \quad \text{where} \quad \begin{array}{l} \phi_i = \dfrac{m_i \pi}{L_x}, \quad \psi_i = \dfrac{n_i \pi}{L_y}, \\ \\ i,j = 1,2, \qquad i \neq j; \end{array} \tag{3.13}$$

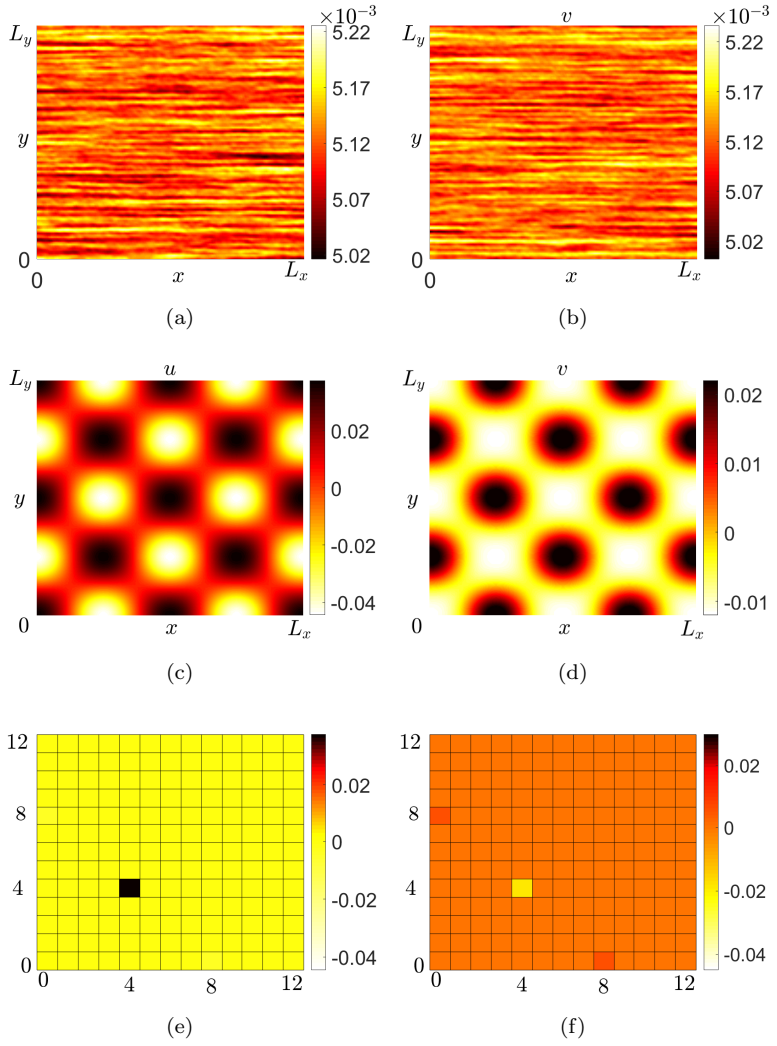

FIGURE 6. Cross-Turing stationary pattern supported by the system (1.1) at a regular bifurcation. The parameters are chosen as $\beta = 0.1$, $\gamma = 1.02$, $\varepsilon = 2$, $a = 0.0001$, so that $E^* = (0.0051, 0.0051)$ and $d_u = 2.035$, $d_v = 0.1$ and $d = 0.2176 < d_c^- \approx 0.2198$. In the square domain $[0, 4\sqrt{2}\pi/k_c] \times [0, 4\sqrt{2}\pi/k_c]$ the Turing bifurcation is regular: the critical wavenumber $k_c \approx 1.2356$ corresponds to the unique couple of modes $(m, n) = (4, 4)$ satisfying the condition (3.11). (a)-(b) Initial condition assigned as a small random perturbation of the homogeneous equilibrium. (b)-(c) Numerical solution of the system (1.1) computed via spectral methods. (d)-(e) Spectrum of the solution.

iv) the following amplitudes system:

$$\begin{aligned} \frac{dA_1}{dT_2} &= \sigma_1 A_1 - L_1 A_1^3 + \Omega_1 A_1 A_2^2 \\ \frac{dA_2}{dT_2} &= \sigma_2 A_2 - L_2 A_2^3 + \Omega_2 A_1^2 A_2 \end{aligned} \tag{3.14}$$

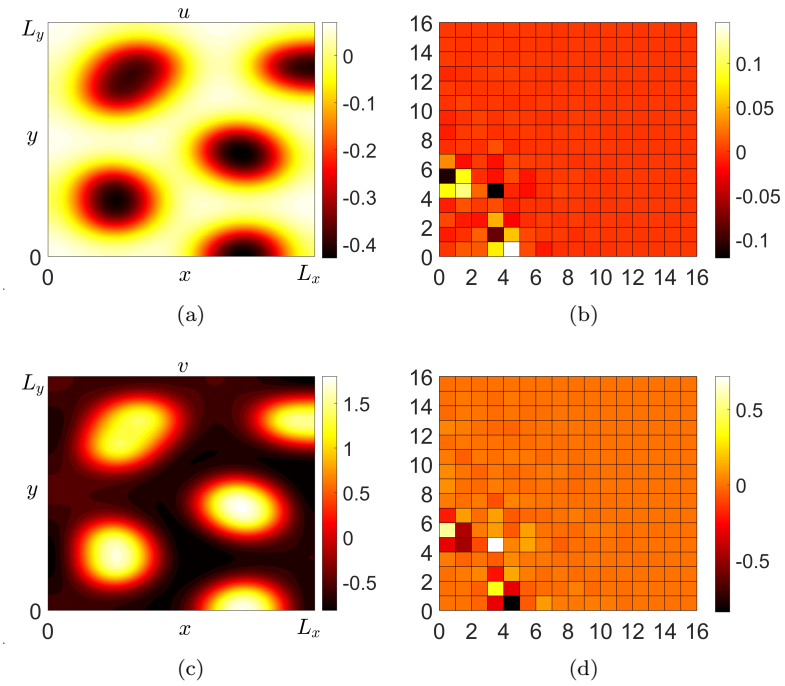

FIGURE 7. Cross-Turing stationary subcritical pattern supported by the system (1.1) at a regular bifurcation. The parameters of the reaction term are chosen as in Fig.6 and $d_v = 0.1$, $d_u = 2.0151$, $d = 0.2024 < d_c^- \approx 0.2026$. In the square domain $[0, \pi] \times [0, \sqrt{2}\pi]$ the most unstable mode $k_c \approx 2.4495$ corresponds to the unique couple of integers $(m, n) = (2, 2)$ satisfying the condition (3.11). The simulation reveals that several modes, other than the critical one, are excited. (a)-(c) Numerical solution of the system (1.1) computed using spectral methods and assigning as initial condition a small random perturbation of the homogeneous equilibrium. (b)-(d) Spectrum of the solution.

admits at least one stable equilibrium. The coefficients of the system (3.14) *are computed in terms of the parameters of the system* (1.1) *through the WNL analysis* [16]*;*

then the asymptotic solution of the system (1.1) *on a two-dimensional rectangular domain* Ω *approximated at the leading order is:*

$$\mathbf{w} = \mu \boldsymbol{\varrho} \left(A_{1\infty} \cos(\phi_1 x) \cos(\psi_1 y) + A_{2\infty} \cos(\phi_2 x) \cos(\psi_2 y) \right) + O(\mu^2), \tag{3.15}$$

where $(A_{1\infty}, A_{2\infty})$ *is a stable steady state of the system* (3.14)*,* $\boldsymbol{\varrho}$ *is given in* (3.5)*,* ϕ_i *and* ψ_i*,* $i = 1, 2$ *are defined as in* (3.10)-(3.11)*.*

The details of the analysis leading to the system (3.14) and the study of the stability of the corresponding equilibria are similar to what has been done in [15] and we will not report them.

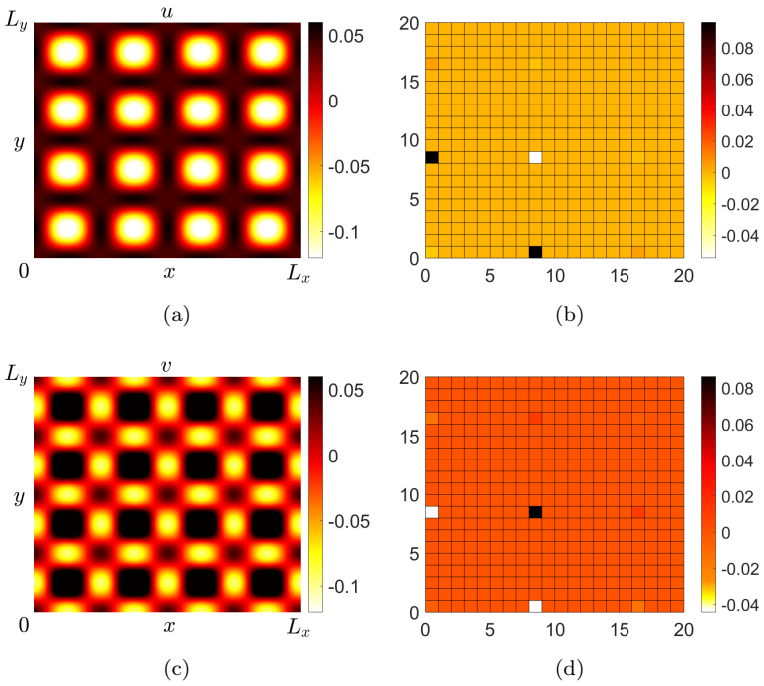

FIGURE 8. Cross-Turing stationary mixed-mode pattern supported by the system (1.1) when the monostable equilibrium loses stability via a degerate bifurcation and non-resonance conditions (3.13) hold. The parameters of the reaction term are chosen as in Fig.6 and $d_u = 2.035$ and $d_v = 0.1$, $d = 0.219 < d_c^- \approx 0.2198$. In the rectangular domain $[0, 8\pi/k_c] \times [0, 8\pi/k_c]$ the most unstable mode $k_c \approx 1.2356$ corresponds to the two couples of integers $(m_1, n_1) = (0, 8)$ and $(m_2, n_2) = (8, 0)$ satisfying the condition (3.11). (a)-(c) Numerical solution of the system (1.1) computed using spectral methods and assigning as initial condition a small random perturbation of the homogeneous equilibrium. (b)-(d) Spectrum of the solution.

A representative cross-Turing mixed-mode pattern of (1.1), as given by (3.15), is shown in Fig.8, where the system parameters are chosen so that the hypotheses of Theorem 2.1 (competition regime, namely $\delta_u^{(1)} \leq d_u \leq \delta_u^{(3)}$, and cross-Turing bifurcation) and the conditions $i) - iv)$ of Case 2 are satisfied. With the chosen parameter set, there exist the two mode pairs $(8, 0)$ and $(0, 8)$ satisfying the conditions (3.11) in the square domain $[0, \frac{8\pi}{k_c}] \times [0, \frac{8\pi}{k_c}]$. The expected solution, computed as in (3.15), is the following superposition of orthogonal stripes:

$$\mathbf{w} = \mu \boldsymbol{\varrho} \left(A_{1\infty} \cos(k_c x) + A_{2\infty} \cos(k_c y) \right) + O(\mu^2), \tag{3.16}$$

with $(A_{1\infty}, A_{2\infty}) \approx (0.3641, 0.3641)$, unique stable equilibrium of the amplitude system (3.14). The expression (3.16) approximates, at the leading order, the solution of the full system (1.1). The mode $(8,8)$ appearing in the spectrum of the solutions is a subharmonic mode which could be predicted at $O(\mu^2)$.

CASE 3 (Resonant):
Asymptotic solution at a degenerate Turing bifurcation in the neighborhood of a monostable equilibrium, resonant case.
Given the system (1.1), let $E^* = (u^*, v^*)$ be the monostable h.s.s. of the system. Let E^* be stable against spatially homogeneous perturbations and let E^* undergo a diffusive bifurcation at $d = d_c$. If:

i) the distance μ from the bifurcation value is small enough such that k_c is the only unstable wavenumber admitted by the boundary conditions;
ii) in the rectangular domain $\Omega \equiv [0, L_x] \times [0, L_y]$ there exist two mode pairs of integers $(m_i, n_i), i = 1, 2$ defined as in (3.10) and satisfying condition (3.11);
iii) the following resonance conditions hold:

$$\begin{array}{llll} \phi_i + \phi_j = \phi_j & \text{and} & \psi_i - \psi_j = \psi_j, & \\ & \text{or} & & \text{where} \quad \phi_i = \dfrac{m_i \pi}{L_x}, \quad \psi_i = \dfrac{n_i \pi}{L_y}, \\ \phi_i - \phi_j = \phi_j & \text{and} & \psi_i + \psi_j = \psi_j, & \\ & & & i, j = 1, 2, \qquad i \neq j; \end{array} \tag{3.17}$$

iv) the following amplitudes system:

$$\begin{aligned} \frac{dA_1}{dT} &= \sigma_1 A_1 - L_1 A_1 A_2 + \Omega_1 A_1^3 + \Phi_1 A_1 A_2^2 \\ \frac{dA_2}{dT} &= \sigma_2 A_2 - L_2 A_1^2 + \Omega_2 A_2^3 + \Phi_2 A_1^2 A_2 \end{aligned} \tag{3.18}$$

admits at least one stable equilibrium. The coefficients of the system (3.18) are computed in terms of the parameters of the system (1.1) through a WNL analysis at $O(\varepsilon^3)$ [16].

Then the emerging solution of the system (1.1) on a two-dimensional rectangular domain Ω approximated at the leading order is:

$$\mathbf{w} = \mu \boldsymbol{\varrho} \left(A_{1\infty} \cos(\phi_1 x) \cos(\psi_1 y) + A_{2\infty} \cos(\phi_2 x) \cos(\psi_2 y) \right) + O(\mu^2), \tag{3.19}$$

where $(A_{1\infty}, A_{2\infty})$ is a stable state of the system (3.18), $\boldsymbol{\varrho}$ is given in (3.5), ϕ_i and ψ_i are defined as in (3.10)-(3.11).

Due to the resonant conditions (3.17), the solution (3.19) describes rolls (when $A_{1\infty} = 0$ and $A_{2\infty} \neq 0$) or hexagons (when both $A_{1\infty}$ and $A_{2\infty}$ are non-zero), see [16] for details. In Fig.9 we report the bifurcation diagram of the amplitude system (3.18) when the control parameter d is close to the cross-Turing bifurcation threshold d_c^-. As the control parameter decreases, the homogeneous steady state loses stability at the primary bifurcation point, labeled by B_p, where two subcritical branches of equilibria, denoted by $H_u^{\pm}$, bifurcate: the two branches, corresponding to hexagons patterns of the FHN system (1.1), have opposite values of A_1 and the same (negative) value of A_2. At the onset, the hexagons $H_u^{\pm}$ arise unstable and gain stability in two saddle-node bifurcations that take place for a common value of d (greater than d_c^-), where the two stable branches of hexagons $H_s^{\pm}$ originate. In the interval between d_c^- and the saddle-node bifurcation value, one has bistability

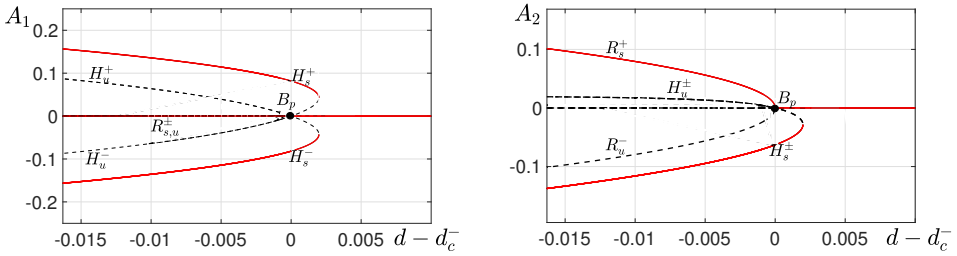

(a) (b)

FIGURE 9. Resonant degenerate cross-Turing bifurcation: bifurcation diagrams of the amplitude system (3.18). The parameters of the reaction term in (1.1) are chosen as in Fig.6 and $d_u = 2.035$ and $d_v = 0.1$, $d_c^- \approx 0.2198$. A solid red (dashed black) line represents stable (unstable) branches of stationary equlibria. The branches labeled by $H_s^{\pm}$ represent stable hexagons of the FHN system (1.1) that bifurcate subcritically from the homogeneous equilibrium at the point B_p. A pair of rolls of (1.1) bifurcates at B_p in a saddle-node bifurcation so leading, on the left of B_p, to coexistence of stable rolls and hexagons. (a) Bifurcation diagram of A_1. (b) Bifurcation diagram of A_2.

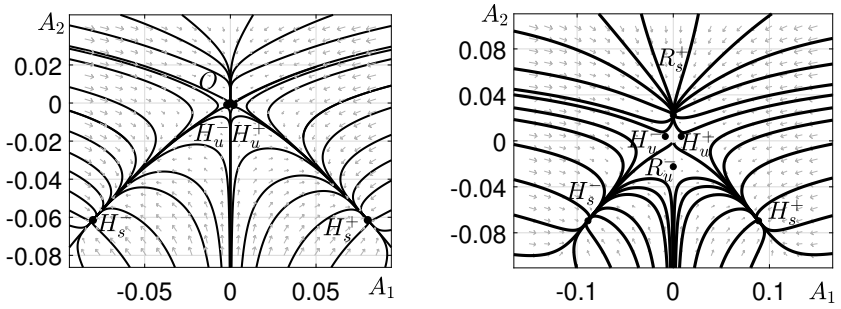

(a) (b)

FIGURE 10. Resonant degenerate cross-Turing bifurcation: phase space diagrams of the amplitude system (3.18). (a) The parameters are chosen as in Fig.9 with $d = d_c^- + 0.0002 = 0.22$. The coordinates of equilibrium points are $H_s^{\pm} = (\pm 0.0801882, -0.061473)$ (stable), $H_u^{\pm} = (\pm 0.00185716, -0.00094344)$ (unstable). (b) The parameters are chosen as in Fig.9 with $d = d_c^- - 0.0008 = 0.219$. The coordinates of equilibrium points are $R_s^+ = (0, 0.02246)$ (stable), $R_u^- = (0, -0.02246)$ (unstable), $H_s^{\pm} = (\pm 0.088722, -0.06956)$ (stable), $H_u^{\pm} = (\pm 0.003852, 0.008295)$ (unstable).

of the hexagons $H_s^{\pm}$ with the homogeneous steady state: the corresponding phase-space diagram of the amplitude system (3.17) for $d = d_c^- + 0.0002$ is reported

in Fig.10(a), where the unstable points representing $H_u^{\pm}$ are also depicted. At the point B_p, where the homogeneous equilibrium loses stability, a pair of rolls, denoted by R_s^+ and R_u^-, respectively, branch off out of a saddle-node bifurcation. The roll branches R_s^+ (stable) and R_u^- (unstable) have both zero component along A_1 and opposite values of A_2. Therefore, if the bifurcation parameter is chosen on the left of the point B_p, one has bistability of the roll R_s^+ with the hexagons $H_s^{\pm}$: the corresponding phase-space diagram of the amplitude system (3.17) for $d = d_c^- - 0.008$ is shown in Fig.10(b), where the unstable points representing $H_u^{\pm}$ and R_u^- are also plotted. Moreover, in Figs.11-12, we show the snapshots of the cross-Turing hexagons and rolls, respectively, obtained for $d = d_c^- - 0.008$ and for two different choices of the initial condition. Namely, for the chosen parameter set, if the initial values of the amplitudes are chosen so that the corresponding point lies in the basin of attraction of H_s^+, one gets the asymptotic hexagonal cross-Turing pattern shown in Fig.11; if the initial amplitudes are picked within the attraction basin of R_s^+, the solution evolves towards the stationary cross-Turing roll showed in Fig.12.

4. **Conclusions.**

In this paper we have investigated the process of pattern formation driven by linear cross-diffusion in a FHN-type model in the monostable regime. We have proved that the presence of linear cross-diffusion terms enlarges the Turing space, allowing for pattern formation also when the diffusivity ratio is less than unity. Besides, for sufficiently high values of the inhibitor cross-diffusion, it also modifies the classical Turing mechanism, determining the formation of out-of-phase stationary patterns that bifurcate from the homogeneous equilibrium when the diffusivity ratio is *below* a given threshold. Finally, very large values of the inhibitor cross-diffusion determine the existence of a different regime, where the pattern forms independently of the self-diffusivity ratio, whose value discerns between the settlement of in-phase versus out-of-phase stationary structures.

Several questions remain to be addressed: for example, it would be interesting to investigate how the presence of cross-diffusion terms changes the pattern-forming properties of the FHN system in the excitable regime. It is, in fact, well known that, in absence of cross-diffusion, the excitable kinetics of the FHN system prohibits diffusion-driven instability. We believe that the presence of cross-terms could induce new phenomena of biological interest in the description of excitable systems.

Another relevant study pertains the introduction of cross-diffusion term in the FHN system in the bistable regime, namely when the reaction kinetics admits two stable steady states. In absence of cross-diffusion, the analysis in the neighborhood of the codimension-2 Turing-pitchfork bifurcation point presented in [39, 38] allows to capture the large amplitude patterns arising next to the nascent bistability. Besides, when the distance from the Turing-pitchfork codimension-2 equilibrium increases, the nonlinear interaction between the Turing patterns emerging close to each of the two steady states, may give rise to the formation of superlattices and more complex patterns [7, 1, 2]. We believe that the cross-diffusion terms could facilitate the formation of such structures and produce interesting developments.

Since the FHN system (1.1) also exhibits Hopf instability, we plan to investigate and predict the oscillating behavior next to the codimension-2 Turing-Hopf bifurcation point, as in [13].

Finally, we will consider the hyperbolic FHN model in order to analyze how cross-terms modify the mechanisms underlying propagation phenomena [4, 5, 59, 58].

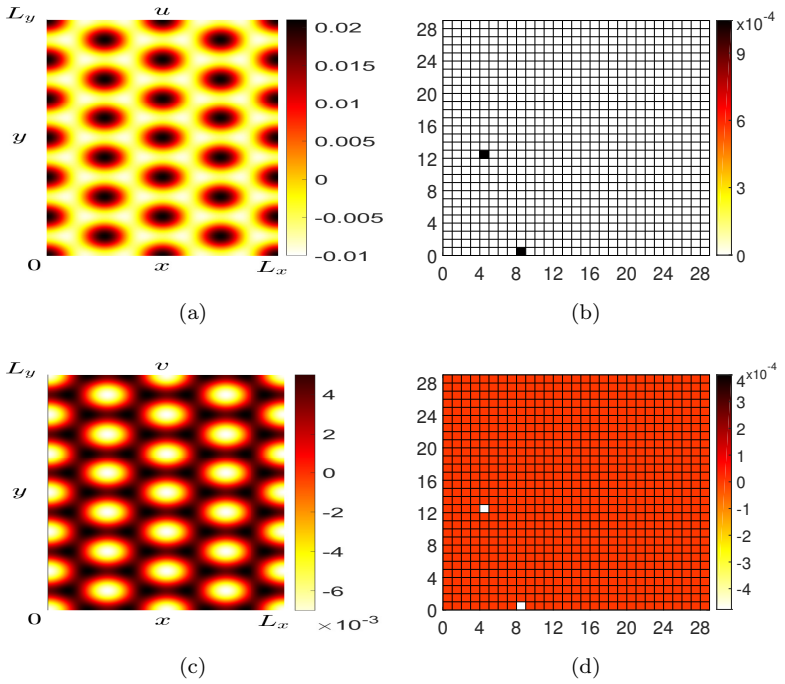

FIGURE 11. Resonant degenerate cross-Turing bifurcation: stationary hexagonal pattern supported by the system (1.1) when resonance conditions (3.17) hold. The parameters are chosen as in Fig.9 with $d = d_c^- - 0.0008 = 0.219$. In the rectangular domain $[0, 8\pi/k_c] \times [0, 8\sqrt{3}\pi/k_c]$ the most unstable mode $k_c \approx 0.8625$ corresponds to the two couples of integers $(m_1, n_1) = (4, 12)$ and $(m_2, n_2) = (8, 0)$ satisfying the condition (3.11). (a)-(c) Numerical solution of the system (1.1) computed using spectral methods. The initial condition is chosen of the form (3.19), where $(A_{1\infty}, A_{2\infty})$ is in the basin of attraction of the stable equilibrium point H_s^+. (b)-(d) Spectrum of the solution.

Appendix A. **Derivation of the FHN system (2.1)-(2.2) from a predator-prey model.** In this Appendix we shall prove that the FHN kinetics of the type given in (2.1)-(2.2) can be derived from the following prey-predator model:

$$\frac{dx}{d\tau} = F(x,y) = x(1-x) - \frac{x}{x+h}y\,, \tag{A.1}$$

$$\frac{dx}{d\tau} = G(x,y) = k\frac{x}{x+h}y - my, \tag{A.2}$$

which describes the dynamics of an aquatic ecosystem, see [35] and references therein. The model (A.1)-(A.2) is a two-species (phytoplankton-zooplankton) system with a logistic local growth of the prey x and a Holling-type II functional response of the predator y. The system is here presented in non-dimensional form (as derived in [35]), so that in the prey equation three parameters are set equal to unity, namely the prey growth rate, the prey carrying capacity and the attack rate

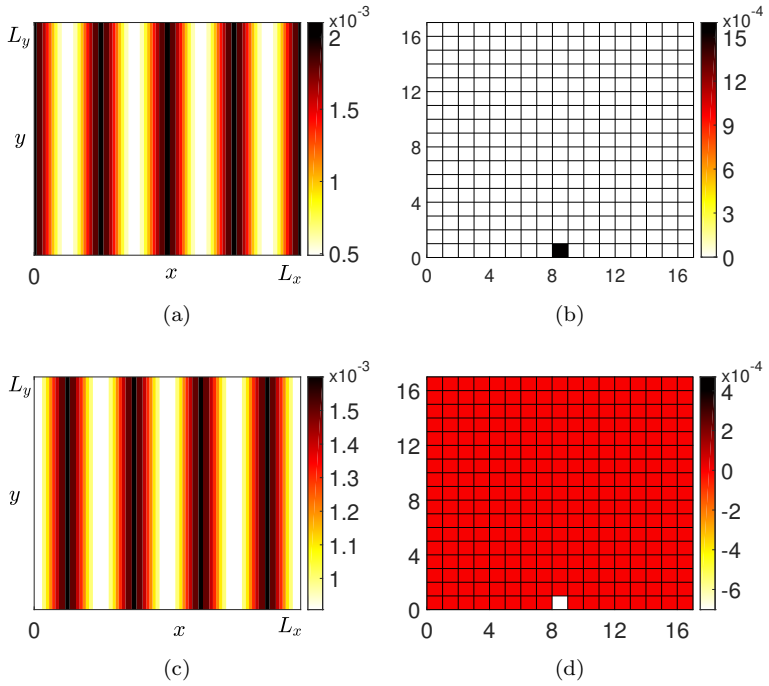

FIGURE 12. Resonant degenerate cross-Turing bifurcation: stationary roll pattern supported by the system (1.1) when resonance conditions (3.17) hold. The parameters and the domain are chosen as in Fig.11. The initial condition is chosen of the form (3.19), where $(A_{1\infty}, A_{2\infty})$ is in the basin of attraction of the stable equilibrium point $R_s^+ = (0, 0.02246)$ and $(m, n) = (8, 0)$. (a)-(c) Numerical solution of the system (1.1) computed via spectral methods. (b)-(d) Spectrum of the solution.

(i.e. the parameter in front of the predation term). In (A.1)-(A.2) the parameter h measures the half-saturation density of the prey, m is the mortality rate of the predator and k is the coefficient of food utilization. In what follows we shall show that the FHN kinetics (2.1)-(2.2) can be interpreted as the reaction terms of a dynamical system that describes the time evolution of the deviations of the species densities (x, y) of (A.1)-(A.2) from the coexistence equilibrium point.
The coordinates of the coexistence equilibrium of (A.1)-(A.2), $C \equiv (x^*, y^*)$, are given by:

$$x^* = \frac{rh}{1-r}, \quad y^* = (1-x^*)(h+x^*), \qquad \text{with} \quad r = \frac{m}{k}. \tag{A.3}$$

The point C is biologically meaningful (i.e. $x^* > 0$ and $y^* > 0$) and stable if the following conditions hold:

$$0 < r < 1 \qquad \text{and} \qquad \frac{1-r}{1+r} < h < \frac{1-r}{r}. \tag{A.4}$$

In the neighborhood of the equilibrium C, one can expand the functions F and G as follows:

$$\begin{aligned} F(x,y) &\simeq \frac{x^*}{x^*+h}\left(1+h\frac{r+1}{r-1}\right)(x-x^*) - \frac{x^*}{x^*+h}(y-y^*) \qquad \text{(A.5)}\\ &+\left(-1+\frac{h(1-x^*)}{(x^*+h)^2}\right)(x-x^*)^2 - \frac{h}{2(x^*+h)^2}(x-x^*)(y-y^*)\\ &-\frac{h(1-x^*)}{(x^*+h)^3}(x-x^*)^3 + \frac{h}{3(x^*+h)^3}(x-x^*)^2(y-y^*)\\ &+\text{higher order terms;} \qquad \text{(A.6)}\\ G(x,y) &\simeq hk\frac{(1-x^*)}{(x^*+h)^2}(x-x^*) + \text{higher order terms,} \end{aligned}$$

where $(x-x^*), (y-y^*)$ measure the small deviations of the populations from the coexistence equilibrium. Our aim is now to suitably rescale the variables in such a way to derive the *canonical* FHN system. Upon defining:

$$X = x - x^* + \alpha_1, \qquad Y = y - y^* + \alpha_2, \qquad \text{(A.7)}$$

through a lengthy but straightforward calculation, one can find α_1 and α_2 such that the system (A.1)-(A.2) reduces to:

$$\begin{aligned} \frac{dX}{d\tau} = F(X,Y) &= c_1X + c_2X^3 + c_3Y + c_4XY + c_5X^2Y\,, \qquad \text{(A.8)}\\ \frac{dY}{d\tau} = G(X,Y) &= c_6X + c_7, \qquad \text{(A.9)} \end{aligned}$$

where the coefficients c_i, $i = 1,\dots,7$ have cumbersome expressions in terms of α_1, α_2 and of the parameters h, k and r, and they will be not reported here. Notice that $F(X,Y)$ in (A.8) presents the same functional form of $f(u,v)$ in (2.1), except for the presence of the term c_5X^2Y. Since (A.8)-(A.9) describes a prey-predator dynamics, provided that $c_4, c_5 < 0$, the term c_5X^2Y models a predation of higher order with respect to the term c_4XY. Therefore, the corresponding term in (2.1), proportional to u^2v, has been neglected. In the function $G(X,Y)$ given in (A.9), the linear term in Y is missing: this means that the Y-nullcline of the system (A.8)-(A.9) is a vertical line. In (2.2) we have chosen to generalize the functional form of the v-nullcline so to let it have a variable slope.

A general discussion of the signs of the coefficients c_i, $i = 1,\dots,7$ in terms of the system parameters h, k and r is an arduous task. Here we just report their values choosing the same parameter set $h = 0.4, r = 0.3, k = 2$ as in the experiments given in [35] (and in the references therein):

$$\begin{aligned} &c_1 = 0.0769,\ c_2 = -10.6575,\ c_3 = -0.3012,\\ &c_4 = -1.2167,\ c_6 = 1.16,\ c_7 = 0.0011. \end{aligned} \qquad \text{(A.10)}$$

Rescaling the variables as follows:

$$t = c_1\tau, \quad u = \sqrt{-\frac{c_2}{c_1}}X, \quad v = -\frac{c_3}{c_1}\sqrt{-\frac{c_2}{c_1}}Y, \qquad \text{(A.11)}$$

the system (A.8)-(A.9), neglecting the cubic term X^2Y, assumes the following *canonical* form:

$$\frac{du}{dt} = u(1-u^2) - v(1-\tilde{\beta}u), \tag{A.12}$$

$$\frac{dv}{dt} = \tilde{\gamma}u - \tilde{a}, \tag{A.13}$$

where:

$$\tilde{\beta} = -0.3431,\ \tilde{\gamma} = 59.0827,\ \tilde{a} = -0.6596. \tag{A.14}$$

Therefore, in the system (A.12)-(A.13) u and v represent the (rescaled) deviations of the prey and the predator species, respectively, from the coexistence equilibrium point and, hence, are not forced to assume non-negative values. Notice that the equilibrium $(u^*, v^*) \equiv (-0.0112, -0.0112)$ of the system (A.12)-(A.13) is such that $u^*, v^* < 0$.

The reaction kinetics (2.1)-(2.2) studied in the paper generalizes (A.12)-(A.13) in that the v-nullcline is a linearly increasing function of u with variable slope.

We stress the fact that our interest is in the relative roles played by the kinetics and cross-diffusion terms regarding the pattern formation mechanisms. For this reason, we have chosen a *canonical*, prototypical form of a simple, cubic reaction term whose linearized kinetics would have the signs given in Fig.1(a) of the paper. In this respect, modifications of the proposed reaction term that do not alter the signs of the linearized matrix, although they will produce quantitative differences, they would not change the pattern formation mechanism highlighted in our study.

Appendix B. **The monostable equilibrium.** In this Appendix we shall derive the conditions under which the system (1.1) admits a unique monostable equilibrium.

The homogeneous steady states of the FHN system (1.1) are the solutions of the following system:

$$\begin{cases} u(1-u^2) - (1-\beta u)v = 0 \\ \gamma u - v - a = 0 \end{cases} \Rightarrow \begin{cases} u^3 - \beta\gamma u^2 + (a\beta + \gamma - 1)u - a = 0 \\ v = \gamma u - a \end{cases}. \tag{B.1}$$

The first equation of the system (B.1) is the following cubic polynomial:

$$u^3 + bu^2 + cu + d = 0, \tag{B.2}$$

where $b = -\beta\gamma$, $c = a\beta + \gamma - 1$ and $d = -a$. Let us first compute its real solution. Putting $u = y - b/3$, the equation (B.2) reads:

$$y^3 + py + q = 0, \tag{B.3}$$

with $p = c - b^2/3$ and $q = b^3/27 - bc/3 + d$.

Defining $y_1, y_2 \in \mathbb{C}$ such that:

$$\begin{cases} y = y_1 + y_2 \\ p = -3y_1y_2 \end{cases} \tag{B.4}$$

the equation (B.3) reduces to:

$$y_1^3 + py + qy_2^3 = -q. \tag{B.5}$$

Therefore y_1 and y_2 are the solutions of the following system:

$$\begin{cases} y_1^3 + y_2^3 = -q \\ y_1y_2 = -\frac{p}{3} \end{cases} \Rightarrow \begin{cases} y_1^3 + y_2^3 = -q \\ y_1^3y_2^3 = -\frac{p^3}{27} \end{cases}, \tag{B.6}$$

or, equivalently, y_1^3 and y_2^3 are the solutions of the following quadratic equation:

$$z^2 + qz - \frac{p^3}{27} = 0. \tag{B.7}$$

The following two cases can be distinguished:

i) $\frac{q^2}{4} + \frac{p^3}{27} \geq 0$.
The solutions of the equation (B.7):

$$z_\pm = -\frac{q}{2} \pm \sqrt{\frac{q^2}{4} + \frac{p^3}{27}} \tag{B.8}$$

are real. Setting $y_1^3 = z_+$ and $y_2^3 = z_-$, we obtain the solution $\tilde{y} \in \mathbb{R}$ of the equation (B.3):

$$\tilde{y} = y_1 + y_2 = \sqrt[3]{z_+} + \sqrt[3]{z_-}. \tag{B.9}$$

ii) $\frac{q^2}{4} + \frac{p^3}{27} < 0$.
The solutions (B.8) are complex, in particular $z_+ = |z_+|e^{i\theta}$ and $z_- = \bar{z}_+ = |z_+|e^{-i\theta}$. Setting $y_1^3 = z_+$ and $y_2^3 = z_-$, we obtain the following complex roots:

$$y_1^{(k)} = \sqrt[3]{|z_+|}e^{i\left(\frac{\theta+2k\pi}{3}\right)} \quad \text{and} \quad y_2^{(k)} = \sqrt[3]{|z_+|}e^{i\left(\frac{-\theta+2k\pi}{3}\right)}, \qquad k = 0, 1, 2. \tag{B.10}$$

The real solution of the equation (B.3) can be therefore computed as follows:

$$\tilde{y} = y_1^{(0)} + y_2^{(0)} = \sqrt[3]{|z_+|}\left(e^{i\frac{\theta}{3}} + e^{-i\frac{\theta}{3}}\right) = \sqrt[3]{|z_+|}\cos\left(\frac{\theta}{3}\right). \tag{B.11}$$

Thus, the real root of the equation (B.2) is given by:

$$u^* = \tilde{y} - \frac{b}{3}, \tag{B.12}$$

with $\tilde{y}$ computed as in (B.9) and (B.11) in case *i)* and *ii)*, respectively. By the system (B.1) we obtain that $E^* \equiv (u^*, v^*)$, with $v^* = \gamma u^* - a$ is an equilibrium of the FHN system.

In the monostable case the equilibrium E^* must be the unique equilibrium for $u < 1/\beta$, and it must be on the inner branch of the u-nullcline (see definition in Section 2). The existence of the unique equilibrium E^* is ensured by imposing that the equation (B.2), or equivalently the equation (B.3), admits only one real root. Let us write the equation (B.3) as follows:

$$(y - \tilde{y})\mathcal{B}(y) = 0, \qquad \text{with} \qquad \mathcal{B}(y) = y^2 + \tilde{y}y + p + \tilde{y}^2. \tag{B.13}$$

The equation (B.3) admits only one real root if the discriminant of the polynomial $\mathcal{B}(y)$ is negative, which reads:

$$p + 3\tilde{y}^2 > 0. \tag{B.14}$$

Moreover, since E^* should be an inner equilibrium, the following condition on the slope of the u-nullcline (2.3) at the equilibrium must apply:

$$v'(u^*) = \frac{\varepsilon_H}{1 - \beta u^*} > 0, \qquad \text{with} \qquad \varepsilon_H = 1 + \beta v^* - 3u^{*2}. \tag{B.15}$$

Being $1 - \beta u^* > 0$, the condition (B.15) is satisfied if:

$$\varepsilon_H > 0. \tag{B.16}$$

Therefore, the FHN system (1.1) is in the monostable case if the parameters a, β and γ are chosen such that the conditions (B.14) and (B.16) hold.

Appendix C. **The amplitude equation in 1D domain.** In this Section we shall give the details of the derivation of the amplitude equations (3.7). The source term $\mathbf{F}$ of the linear problem (3.6) at $O(\varepsilon^2)$ reads:

$$\mathbf{F} = \frac{\partial \mathbf{w}_1}{\partial T_1} + \begin{pmatrix} 3\mathbf{w}_1(1)^2 u^* - \beta \mathbf{w}_1(1)\mathbf{w}_1(2) \\ -d^{(1)} \dfrac{\partial^2 \mathbf{w}_1(2)}{\partial x^2} \end{pmatrix}, \tag{C.1}$$

where $\mathbf{w}_1(i)$, $i = 1, 2$ is the $i-$th entry of the vector $\mathbf{w}_1$. Once substituted the solution (3.5) in (C.1), the Fredholm alternative is automatically satisfied putting $d^{(1)} = 0$ and $T_1 = 0$. The second order coefficient of the expansion in (3.1) for $\mathbf{w}$ can be therefore computed as follows:

$$\mathbf{w}_2 = A^2 \sum_{i=0,2} \mathbf{w}_{2i} \cos(ik_c x)), \tag{C.2}$$

where the vectors $\mathbf{w}_{2i}$ are the solutions of the following linear systems:

$$K\mathbf{w}_{20} = \frac{1}{2}\begin{pmatrix} 3u^* - \beta M \\ 0 \end{pmatrix}, \qquad (K - 4k_c^2 D^c)\mathbf{w}_{20} = \frac{1}{2}\begin{pmatrix} 3u^* - \beta M \\ 0 \end{pmatrix}. \tag{C.3}$$

The problem at $O(\varepsilon^3)$ reads as follows:

$$\mathcal{L}^{b^c}\mathbf{w}_3 = \mathbf{G}, \tag{C.4a}$$

where

$$\mathbf{G} = \left(\frac{dA}{dT}\boldsymbol{\varrho} + A\mathbf{G}_1^{(1)} + A^3\mathbf{G}_1^{(3)}\right)\cos(k_c x) + A^3\mathbf{G}_3\cos(3k_c x)\,, \tag{C.4b}$$

and

$$\begin{aligned} \mathbf{G}_1^{(1)} &= \begin{pmatrix} 0 \\ d^{(2)}k_c^2 M \end{pmatrix}, \\ \mathbf{G}_1^{(3)} &= \begin{pmatrix} \mathbf{G}_1^{(3)}(1) \\ 0 \end{pmatrix}, \\ \mathbf{G}_3 &= \begin{pmatrix} \dfrac{1}{4} + 3u^*\mathbf{w}_{22}(1) - \dfrac{\beta}{2}(M\mathbf{w}_{22}(1) + \mathbf{w}_{22}(2)) \\ 0 \end{pmatrix}. \end{aligned}$$

where

$$\mathbf{G}_1^{(3)}(1) = \frac{3}{4} + 3u^*(2\mathbf{w}_{20}(1) + \mathbf{w}_{22}(1)) - \frac{\beta}{2}(M\mathbf{w}_{22}(1) + \mathbf{w}_{22}(2) + 2M\mathbf{w}_{20}(1) + 2\mathbf{w}_{20}(2))$$

The solvability condition for the equation (C.4a) leads to the amplitude equation (3.7) for $A(T)$, where the expressions of the coefficients σ and L are given by:

$$\sigma = -\frac{< \mathbf{G}_1^{(1)}, \boldsymbol{\psi} >}{< \boldsymbol{\varrho}, \boldsymbol{\psi} >}, \qquad L = \frac{< \mathbf{G}_1^{(3)}, \boldsymbol{\psi} >}{< \boldsymbol{\varrho}, \boldsymbol{\psi} >}, \tag{C.6}$$

with:

$$\boldsymbol{\psi} = \begin{pmatrix} 1 \\ M^* \end{pmatrix}, \qquad M^* = \frac{k_c^2 - \varepsilon_H}{\varepsilon\gamma - k_c^2 d_u}.$$

Acknowledgments. The authors thank the two anonymous Referees for the comments that greatly helped improve the presentation of the results. This work has been supported by the PRIN grant 2017 "Multiscale phenomena in Continuum Mechanics: singular limits, off-equilibrium and transitions" (project no. 2017YBKNCE). The authors also acknowledge the financial support of GNFM-INdAM.

References

[1] M. Bachir, S. Métens, P. Borckmans and G. Dewel, Formation of rhombic and superlattice patterns in bistable systems, *Europhysics Letters*, **54** (2001), 612–618.

[2] M. Bachir, G. Sonnino and M. Tlidi, Predicted formation of localized superlattices in spatially distributed reaction-diffusion solutions, *Physical Review E*, **86** (2012), 045103.

[3] N. Boudiba and M. Pierre, Global existence for coupled reaction–diffusion systems, *Journal of Mathematical Analysis and Applications*, **250** (2000), 1–12.

[4] G. Consolo, C. Currò and G. Valenti, Pattern formation and modulation in a hyperbolic vegetation model for semiarid environments, *Appl. Math. Model.*, **43** (2017), 372–392.

[5] G. Consolo, C. Currò and G. Valenti, Supercritical and subcritical Turing pattern formation in a hyperbolic vegetation model for flat arid environments, *Physica D: Nonlinear Phenomena*, **398** (2019), 141–163.

[6] A. De Wit, *Spatial Patterns and Spatiotemporal Dynamics in Chemical Systems*, 435–513, John Wiley & Sons, Ltd, 2007.

[7] G. Dewel, M. Bachir, P. Borckmans and S. Métens, Superlattice structures and quasipatterns in bistable systems, *Comptes Rendus de l'Academie de Sciences - Serie IIb: Mecanique*, **329** (2001), 411–416.

[8] G. Dewel, S. Métens, M. Hilali, P. Borckmans and C. B. Price, Resonant patterns through coupling with a zero mode, *Phys. Rev. Lett.*, **74** (1995), 4647–4650.

[9] X. Diego, L. Marcon, P. Müller and J. Sharpe, Key features of Turing systems are determined purely by network topology, *Physical Review X*, **8** (2018), 021071.

[10] E. Dulos, J. Boissonade, J. Perraud, B. Rudovics and P. Kepper, Chemical morphogenesis: Turing patterns in an experimental chemical system, *Acta biotheoretica*, **44** (1996), 249–61.

[11] R. FitzHugh, Thresholds and plateaus in the Hodgkin-Huxley nerve equations., *The Journal of general physiology*, **43** (1960), 867–896.

[12] G. Gambino, M. Lombardo, S. Lupo and M. Sammartino, Super-critical and sub-critical bifurcations in a reaction-diffusion Schnakenberg model with linear cross-diffusion, *Ricerche di Matematica*, **65** (2016), 449–467.

[13] G. Gambino, M. Lombardo, S. Lupo and M. Sammartino, Turing–Hopf bifurcation in the Schnakenberg model with cross-diffusion, *submitted*.

[14] G. Gambino, M. Lombardo, G. Rubino and M. Sammartino, Pattern selection in the 2D Fitzhugh-Nagumo model, *Ricerche di Matematica*, **68** (2019), 535–549.

[15] G. Gambino, M. Lombardo and M. Sammartino, Turing instability and traveling fronts for a nonlinear reaction–diffusion system with cross–diffusion, *Mathematics and Computers in Simulation*, **82** (2012), 1112 – 1132.

[16] G. Gambino, M. Lombardo and M. Sammartino, Pattern formation driven by cross-diffusion in a 2D domain, *Nonlinear Analysis: Real World Applications*, **14** (2013), 1755–1779.

[17] G. Gambino, M. Lombardo and M. Sammartino, Cross-diffusion-induced subharmonic spatial resonances in a predator-prey system, *Physical Review E*, **97** (2018), 012220.

[18] X. Gao, L. Dong, H. Wang, H. Zhang, Y. Liu, W. Liu, W. Fan and Y. Pan, Three-dimensional patterns in dielectric barrier discharge with "h" shaped gas gap, *Physics of Plasmas*, **23** (2016), 083526.

[19] A. Gierer and H. Meinhardt, A theory of biological pattern formation, *Kybernetik*, **12** (1972), 30–39.

[20] A. Hagberg and E. Meron, Pattern formation in non-gradient reaction-diffusion systems: The effects of front bifurcations, *Nonlinearity*, **7** (1994), 805–835.

[21] R. Han and B. Dai, Spatiotemporal pattern formation and selection induced by nonlinear cross-diffusion in a toxic-phytoplankton-zooplankton model with Allee effect, *Nonlinear Analysis: Real World Applications*, **45** (2019), 822–853.

[22] M. Haragus and G. Iooss, *Local bifurcations, center manifolds, and normal forms in infinite-dimensional dynamical systems*, Universitext, Springer-Verlag London, Ltd., London; EDP Sciences, Les Ulis, 2011.

[23] B. Henry and S. Wearne, Existence of Turing instabilities in a two-species fractional reaction-diffusion system, *SIAM Journal on Applied Mathematics*, **62** (2002), 870–887.

[24] J. Horváth, I. Szalai and P. De Kepper, An experimental design method leading to chemical Turing patterns, *Science*, **324** (2009), 772–775.

[25] J. Irazoqui, A. Gladfelter and D. Lew, Scaffold-mediated symmetry breaking by Cdc42p, *Nature Cell Biology*, **5** (2003), 1062–1070.

[26] D. Karig, K. Michael Martini, T. Lu, N. DeLateur, N. Goldenfeld and R. Weiss, Stochastic Turing patterns in a synthetic bacterial population, *Proceedings of the National Academy of Sciences of the United States of America*, **115** (2018), 6572–6577.
[27] A. Landge, B. Jordan, X. Diego and P. Müller, Pattern formation mechanisms of self-organizing reaction-diffusion systems, *Developmental Biology*, **460** (2020), 2–11.
[28] B. Liu, R. Wu and L. Chen, Patterns induced by super cross-diffusion in a predator-prey system with Michaelis-Menten type harvesting, *Mathematical Biosciences*, **298** (2018), 71–79.
[29] M. Loose, E. Fischer-Friedrich, J. Ries, K. Kruse and P. Schwille, Spatial regulators for bacterial cell division self-organize into surface waves in vitro, *Science*, **320** (2008), 789–792.
[30] A. Madzvamuse and R. Barreira, Domain-growth-induced patterning for reaction-diffusion systems with linear cross-diffusion, *Discrete & Continuous Dynamical Systems - B*, **23** (2018), 2775–2801.
[31] A. Madzvamuse, H. Ndakwo and R. Barreira, Stability analysis of reaction-diffusion models on evolving domains: The effects of cross-diffusion, *Discrete & Continuous Dynamical Systems*, **36** (2016), 2133–2170.
[32] A. Madzvamuse, H. Ndakwo and R. Barreira, Cross-diffusion-driven instability for reaction-diffusion systems: analysis and simulations, *Journal of Mathematical Biology*, **70** (2014), 709–743.
[33] B. J. Matkowsky, Nonlinear dynamic stability: A formal theory, *SIAM Journal on Applied Mathematics*, **18** (1970), 872–883.
[34] G. Maugin, *The Thermomechanics of Nonlinear Irreversible Behaviours*, vol. 27, World Scientific Series in Nonlinear Science, Singapore, 1999.
[35] A. Medvinsky, S. Petrovskii, I. Tikhonova, H. Malchow and B.-L. Li, Spatiotemporal complexity of plankton and fish dynamics, *SIAM Review*, **44** (2002), 311–370.
[36] H. Meinhardt, Turing's theory of morphogenesis of 1952 and the subsequent discovery of the crucial role of local self enhancement and long-range inhibition, *Interface Focus*, **2** (2012), 407–416.
[37] V. Mendez, W. Horsthemke, E. P. Zemskov and J. C. Vazquez, Segregation and pursuit waves in activator-inhibitor systems, *Physical Review E*, **76** (2007), 046222.
[38] S. Métens, P. Borckmans and G. Dewel, Large amplitude patterns in bistable reaction-diffusion systems, in *Instabilities and Nonequilibrium Structures VI. Nonlinear Phenomena and Complex Systems* (eds. E. Tirapegui, J. Martinez and R. Tiemann), vol. 5, Springer, Dordrecht, 2000, 153–163.
[39] S. Métens, G. Dewel, P. Borckmans and R. Engelhardt, Pattern selection in bistable systems, *Europhysics Letters*, **37** (1997), 109–114.
[40] J. D. Murray, *Mathematical Biology*, vol. I & II, 3rd edition, Springer, New York, 2007.
[41] J. Nagumo, S. Arimoto and S. Yoshizawa, An active pulse transmission line simulating nerve axon, *Proceedings of the IRE*, **50** (1963), 2061–2070.
[42] A. Nepomnyashchy, Mathematical modelling of subdiffusion-reaction systems, *Mathematical Modelling of Natural Phenomena*, **11** (2016), 26–36.
[43] M. Pierre, Global existence in reaction-diffusion systems with control of mass: a survey, *Milan Journal of Mathematics*, **78** (2010), 417–455.
[44] H.-G. Purwins, H. Bodeker and S. Amiranashvili, Dissipative solitons, *Advances in Physics*, **59** (2010), 485–701.
[45] J. Rauch and J. Smoller, Qualitative theory of the Fitzhugh-Nagumo equations, *Advances in Mathematics*, **27** (1978), 12–44.
[46] K. Schoenbach, M. Moselhy and W. Shi, Self-organization in cathode boundary layer microdischarges, *Plasma Sources Science and Technology*, **13** (2004), 177–185.
[47] A. Sih, The behavioral response race between predator and prey, *The American Naturalist*, **123** (1984), 143–150.
[48] J. Smoller, *Shock Waves and Reaction-Diffusion Equations*, vol. 258, 2nd edition, Springer-Verlag New York, NY, 1994.
[49] E. Tulumello, M. Lombardo and M. Sammartino, Cross-diffusion driven instability in a predator-prey system with cross-diffusion, *Acta Applicandae Mathematicae*, **132** (2014), 621–633.
[50] A. M. Turing, The chemical basis of morphogenesis, *Philosophical Transactions of the Royal Society B: Biological Sciences*, **237** (1952), 37–72.

[51] R. Van Gorder, V. Klika and A. Krause, Turing conditions for pattern forming systems on evolving manifolds, *Journal of Mathematical Biology*, **82** (2021), 4.
[52] V. Vanag and I. Epstein, Cross-diffusion and pattern formation in reaction-diffusion systems, *Physical Chemistry Chemical Physics*, **11** (2009), 897–912.
[53] A. Winfree, Varieties of spiral wave behavior: An experimentalist's approach to the theory of excitable media, *Chaos*, **1** (1991), 303–334.
[54] T. Woolley, R. Baker, E. Gaffney and P. Maini, Stochastic reaction and diffusion on growing domains: Understanding the breakdown of robust pattern formation, *Physical Review E*, **84** (2011), 046216.
[55] T. Woolley, A. Krause and E. Gaffney, Bespoke Turing systems, *Bulletin of Mathematical Biology*, **83** (2021), 41.
[56] M. Zaidi, S. Bendoukha and S. Abdelmalek, Global existence of solutions for an m-component cross-diffusion system with a 3-component case study, *Nonlinear Analysis: Real World Applications*, **45** (2019), 262–284.
[57] E. Zemskov, I. Epstein and A. Muntean, Oscillatory pulses in Fitzhugh-Nagumo type systems with cross-diffusion, *Mathematical Medicine and Biology*, **28** (2011), 217–226.
[58] E. Zemskov and W. Horsthemke, Diffusive instabilities in hyperbolic reaction-diffusion equations, *Physical Review E*, **93** (2016), 032211.
[59] E. Zemskov, M. Tsyganov and W. Horsthemke, Wavy fronts in a hyperbolic Fitzhugh-Nagumo system and the effects of cross diffusion, *Physical Review E*, **91** (2015), 062917.
[60] E. Zemskov, M. Tsyganov and W. Horsthemke, Oscillatory pulses and wave trains in a bistable reaction-diffusion system with cross diffusion, *Physical Review E*, **95** (2017), 012203.
[61] E. Zemskov, M. Tsyganov and W. Horsthemke, Oscillatory multipulsons: Dissipative soliton trains in bistable reaction-diffusion systems with cross diffusion of attractive-repulsive type, *Physical Review E*, **101** (2020), 032208.
[62] E. Zemskov, M. Tsyganov, K. Kassner and W. Horsthemke, Nonlinear waves in a quintic Fitzhugh-Nagumo model with cross diffusion: Fronts, pulses, and wave trains, *Chaos*, **31** (2021), 033141.
[63] Q. Zheng and J. Shen, Pattern formation in the Fitzhugh-Nagumo model, *Computers and Mathematics with Applications*, **70** (2015), 1082–1097.

Received xxxx 20xx; revised xxxx 20xx.

E-mail address: gaetana.gambino@unipa.it
E-mail address: v.giunta@sheffield.ac.uk
E-mail address: mariacarmela.lombardo@unipa.it
E-mail address: gianfranco.rubino@live.it